

# Coupled Natural Gas and Electric Power Systems

Abhi Ojha

Thesis submitted to the Faculty of the  
Virginia Polytechnic Institute and State University  
in partial fulfillment of the requirements for the degree of

Master of Science

in

Electrical Engineering

Vassilis Kekatos, Chair

Lamine M. Mili

Virgilio A. Centeno

June 28, 2017

Blacksburg, Virginia

Keywords: Successive convex approximation, semidefinite programming, feasible point  
pursuit, alternating direction method of multipliers

Copyright 2017

# Coupled Natural Gas and Electric Power Systems

Abhi Ojha

(ABSTRACT)

Decreasing gas prices and the pressing need for fast-responding electric power generators are currently transforming natural gas networks. The intermittent operation of gas-fired plants to balance wind generation introduces spatiotemporal fluctuations of increasing gas demand. At the heart of modeling, monitoring, and control of gas networks is a set of nonlinear equations relating nodal gas injections and pressures to flows over the pipelines. Given gas demands at all points of the network, the gas flow task aims at finding the rest of the physical quantities. This problem is posed here as a feasibility problem involving quadratic equalities and inequalities, and is further relaxed to a convex semidefinite program (SDP) minimization. Drawing parallels to the power flow problem, the relaxation is shown to be exact if the cost function is judiciously designed using a representative set of network states. Adding to the complexity of gas flow task, this thesis also considers the coupled dynamic and natural gas and electric power systems. The optimal dispatch problem is posed as a relaxed convex minimization problem, which is solved using the feasible point pursuit (FPP) algorithm. For a decentralized solution, alternating direction method of multipliers (ADMM) is used in collaboration with the FPP. Numerical experiments conducted on a Belgian gas network coupled with the IEEE 14 bus benchmark system corroborate significant enhancements on computational efficiency compared with the centralized FPP based approach.

# Coupled Natural Gas and Electric Power Systems

Abhi Ojha

(GENERAL AUDIENCE ABSTRACT)

The increase in penetration of renewable energy in the electric power grid has led to increased fluctuations in the power. The conventional coal based generators are inept to handle these fluctuations and thus, natural gas generators, which have fast response times are used to handle the intermittency caused by renewable energy sources. This manuscript solves the problem of finding the optimal dispatch of coupled natural gas and electric power systems. First, the optimal dispatch problem is framed as a optimization problem and then mathematical solvers are developed. Using the mathematical tools of Feasible point pursuit and Alternating direction method of multipliers, a distributed solver is developed, which can solve the optimal dispatch for large power and natural gas networks. The proposed algorithm is tested on a part of a Belgian gas network and the IEEE 14 bus power system. The algorithm is shown to converge to a feasible point.

# Acknowledgments

First and foremost, I would like to thank my research advisor Dr. Vassilis Kekatos for accepting me in his research group at Virginia Tech. Dr. Kekatos helped me develop a strong mathematical background and allowed me to chose my own research area. He also taught me *Power system operation and control*, which was most useful for my research. The doors of his office were always open for me and he helped me throughout my Master's degree.

I would also like to thank Dr. Lamine Mili and Dr. Virgilio A. Centeno for agreeing to be a part of my thesis committee. Dr. Centeno was my interim advisor when I moved to Virginia Tech and he helped me find the right research area. He was the first one to guide me and show me the Power Lab at Virginia Tech. Dr. Mili taught me *Advanced topics in Power Systems* and *Computation methods in Power Systems*. Both of these courses helped me in pursuing my research. He always explained topics in great detail and his classes were one of the best classes I took at Virginia Tech.

Finally, I would like to thank my parents and my sister for their constant support and encouragement.

# Contents

<b>1</b>	<b>Introduction</b>	<b>1</b>
1.1	Natural gas systems . . . . .	2
1.2	Electric power systems . . . . .	5
1.3	Literature review . . . . .	6
<b>2</b>	<b>Background</b>	<b>10</b>
2.1	Semi-definite programming . . . . .	10
2.2	Feasible point pursuit . . . . .	11
2.3	Alternating direction method of multipliers . . . . .	12
<b>3</b>	<b>Steady-state gas flow</b>	<b>15</b>
3.1	Introduction . . . . .	15
3.2	Natural gas network modeling . . . . .	16

3.3	Semidefinite program relaxation (SDR).....	22
3.4	Objective function design .....	26
3.5	An alternative approach .....	33
3.6	Numerical tests .....	35
3.7	Conclusions .....	40
<b>4.</b>	<b>Optimal dispatch of coupled electricity and natural gas networks</b>	<b>44</b>
4.1	Introduction .....	44
4.2	Problem statement .....	45
4.3	Feasible point pursuit-based solver .....	51
4.4	Distributed algorithm .....	53
4.5	Numerical tests .....	58
4.6	Conclusions .....	62
	<b>Bibliography</b>	<b>65</b>

# List of Figures

1.1	Conventional deposits of natural gas. . . . .	3
1.2	Major natural gas transportation corridors in the USA [1]. . . . .	4
1.3	natural gas market centers in the USA [1]. . . . .	5
1.4	Electric power system [2]. . . . .	6
1.5	Independent system operators in the US. . . . .	7
3.1	Gas network pipeline $(i, j)$ . . . . .	17
3.2	Gas network pipeline $(i, j)$ with compressor. . . . .	19
3.3	Modified Belgian gas network [3]. . . . .	36
3.4	Belgian gas network [4]. . . . .	37
3.5	Injection variability for perturbing nodal gas pressures by $\zeta = 0.5$ (top) and $\zeta = 1.0$ (bottom). . . . .	42
3.6	Probability of success for Newton-Raphson and the SDR schemes. . . . .	43

3.7	Probability of success for the alternative SDR scheme. . . . .	43
4.1	Gas network segments. . . . .	47
4.2	Overlapping between different areas. . . . .	55
4.3	Coupled gas and power system network. Red and yellow arrows indicate gas flow from the gas network to the gas fired generator connected to the power network. . . . .	59
4.4	Gas demand profiles. . . . .	60
4.5	Gas demand profiles. . . . .	61
4.6	Convergence plot for FPP algorithm. . . . .	62
4.7	a) Gas flow out of node 16 of the gas network. b) Power generator by the gas-fired generator at node 16 of the gas network . . . . .	63
4.8	Pressure at gas power nodes. . . . .	64

# List of Tables

3.1 Pipeline Description . . . . .	38
3.2 Nominal & Perturbed Gas Pressures and Injections . . . . .	41

# Chapter 1

## Introduction

Natural gas is currently at the core of the energy discussion. Due to the hydro-fracking technology, substantial supplies of natural gas are being discovered [5]. The substitution of oil by natural gas is primarily determined by the ratio of oil to natural gas prices. Granted the increasing trends of oil prices in the US, natural gas is becoming more economically appealing. Its role is likely to expand further in carbon-constrained electric power systems with higher penetration of renewables as the variability of wind generation complements well with gas-fired power plants offering fast-responding reserves [6].

Natural gas is transported from source sites to electricity generators and other loads over a continent-wide network of pipelines. To alleviate the pressure drop across pipelines, compressors are routinely used to boost pressure up to desirable levels. Gas distribution companies typically withdraw gas with low intra-day variation and enter into long-term firm contracts

with gas transmission companies [7]. Under this setup, gas networks have been adequately captured using steady-state gas models. However, if larger volumes of gas are consumed by gas-fired power plants, the intermittency of renewable electric energy resources may translate to higher variability in gas demand [8]. Moreover, congestion in gas networks may force power system operators committing more expensive generators. This upcoming mode of operation necessitates computational tools for dispatching natural gas networks in tandem with power systems and under more dynamic conditions.

## 1.1 Natural gas systems

Natural gas systems perform the primary function of transporting natural gas, primarily methane, from producers to end consumers. In the production phase, holes are drilled into the ground to reach the natural gas deposits. A wellhead is then employed to extract the gas from underground. Recent advancements in the field of natural gas extraction have led to horizontal drilling techniques and hydraulic fracking, which has enabled recovery of natural gas trapped under shale rock formations. Figure 1.1 shows the various types of conventional deposits of natural gas.

The flow of natural gas in a pipeline is determined by the pressure difference between its two points. Since reliable operation of natural gas networks requires pressures to be within specific ranges, compressor stations are installed throughout the network to monitor and control the pressure. In contrast to the power systems having conventional coal-based generators,

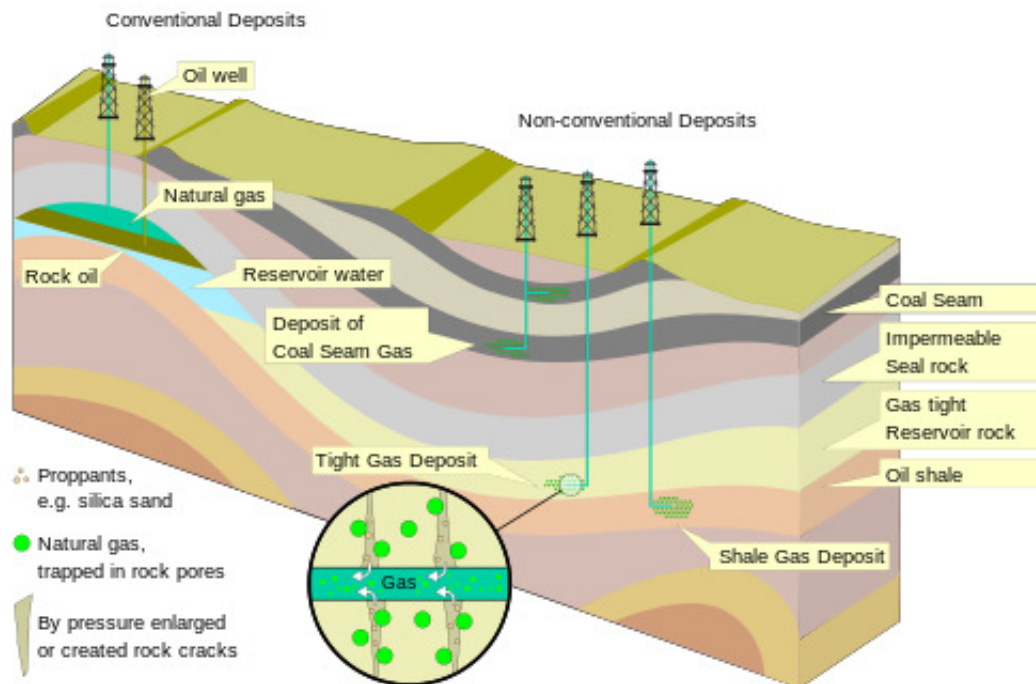


Figure 1.1: Conventional deposits of natural gas.

natural gas systems can manage demand supply imbalances as the gas can be stored in the pipelines. Figure 1.2 major natural gas transportation corridors in the USA, for a detailed report see [1] for a detailed report.

Unlike the ISO's for power transmission networks in the USA, gas transmission networks do not have a centralized system operator. Most transactions in the gas network occur as bilateral arrangements between the shipping and the receiving party. Large consumers such as industrial users directly connect to high pressure gas pipelines and make their own shipping arrangements, while small residential consumers receive their gas through utility companies.

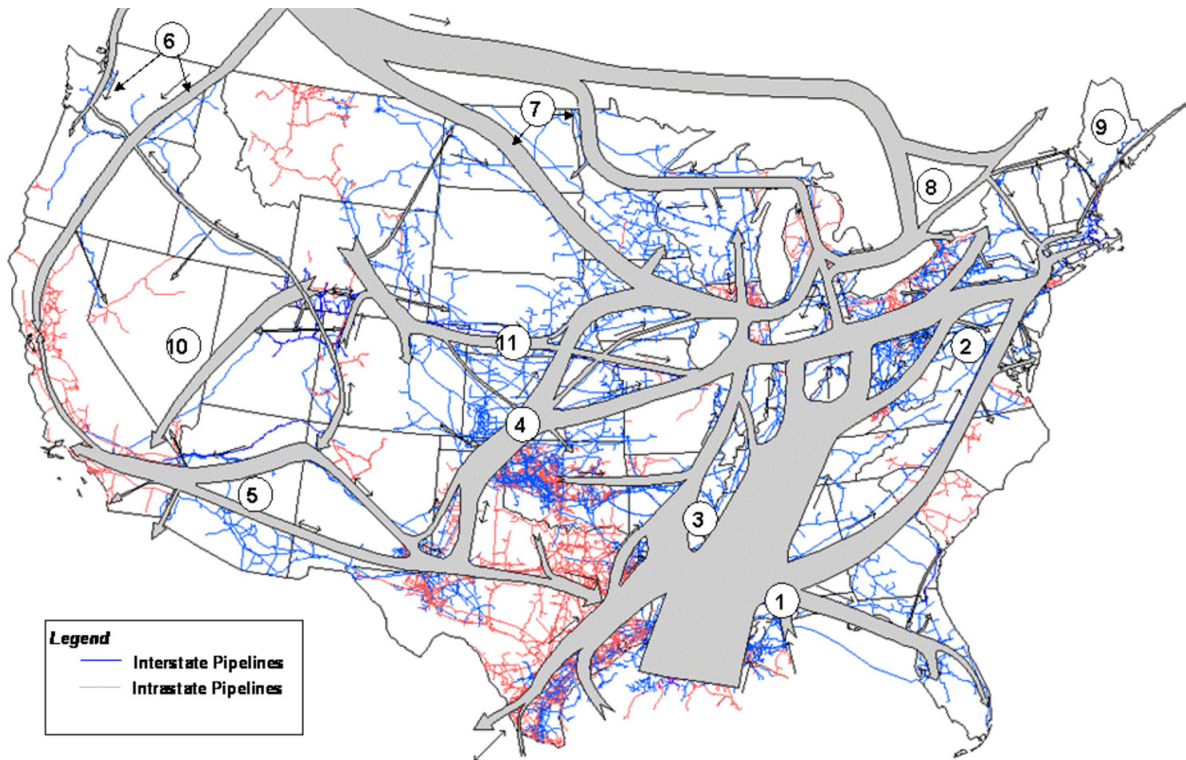


Figure 1.2: Major natural gas transportation corridors in the USA [1].

Currently in the USA, gas pipeline operators are responsible for investing in new pipelines after taking approval from the Federal Energy Regulatory Commission (FERC). Capacity rights of various time durations along with availability guarantees are auctioned to gas producers or consumers [9]. The cost of natural gas is a sum of the commodity and transportation costs. The commodity cost is the price of natural gas at Henry Hub, which is a location in the USA where many pipelines meet [9], see Fig. 1.3. The transportation cost is the price difference between Henry Hub and any other hub in the country. Natural gas markets have a single-day trading with multiple intraday changes to balance supply and demand.

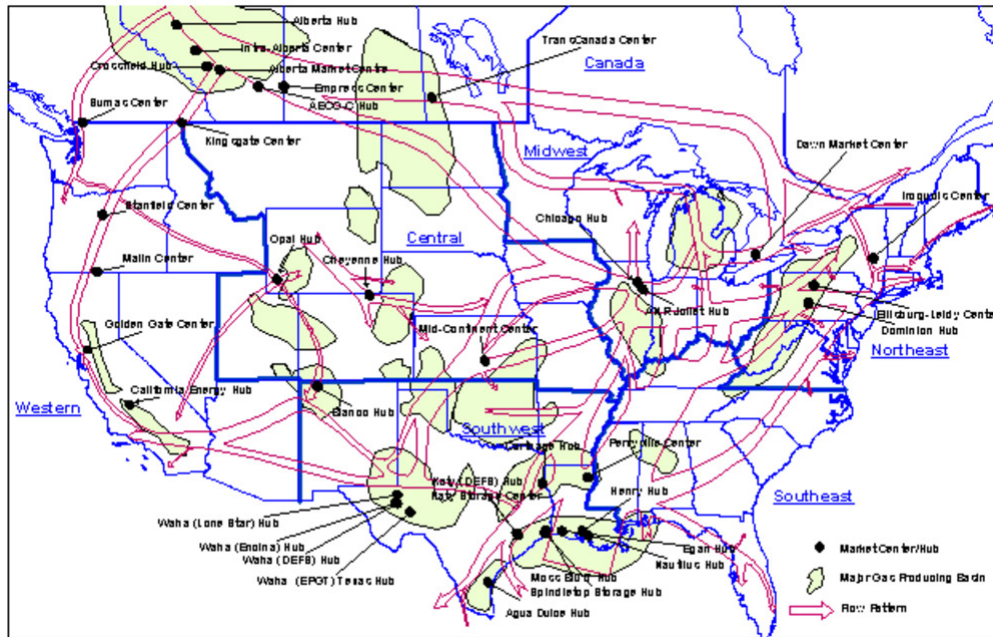


Figure 1.3: natural gas market centers in the USA [1].

## 1.2 Electric power systems

Electric power systems perform the function of delivering power from generators to end consumers. They consist of generating stations, high-voltage transmission networks, medium- and low-voltage distribution grids, all connected through substations as shown in Fig. 1.4. Transformers in electric grids perform the function of transforming high-voltage electricity to low-voltage. The low-voltage distribution lines help in distributing electricity to end consumers.

The electric power grid in the US is partitioned into several reliability areas and/or independent system operators as shown in Fig. 1.5. ISOs are responsible for coordinating system and market activities between producers and consumers. Large-scale industrial customers

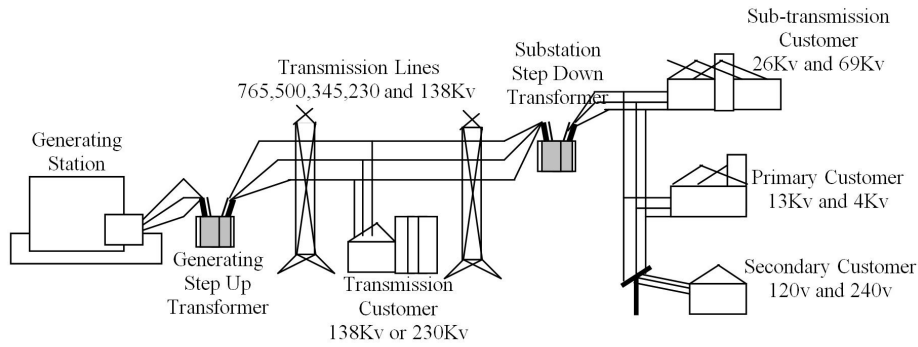


Figure 1.4: Electric power system [2].

and utilities may connect directly to the high-voltage transmission network, while residential customers get their electricity from the utilities. Each ISO collects bids from electric power generators and consumers through a day-ahead and real-time market. After dispatching the grid in the most economical fashion while respecting transmission network limitations, the ISO announces the price for buying and selling electricity at every node of the power system. For a detailed review of whole-sale electricity markets, see [10].

### 1.3 Literature review

The review of computational advances in gas networks commences with the gas flow (GF) problem. Given gas injections and pressures at specific network nodes, the GF task aims at solving the equations describing gas flows. In a network without compressors, the flows and pressures can be recovered as the primal-dual solutions of a convex problem [11]. For general networks, the GF task can be solved using the Newton-Raphson method, yet its

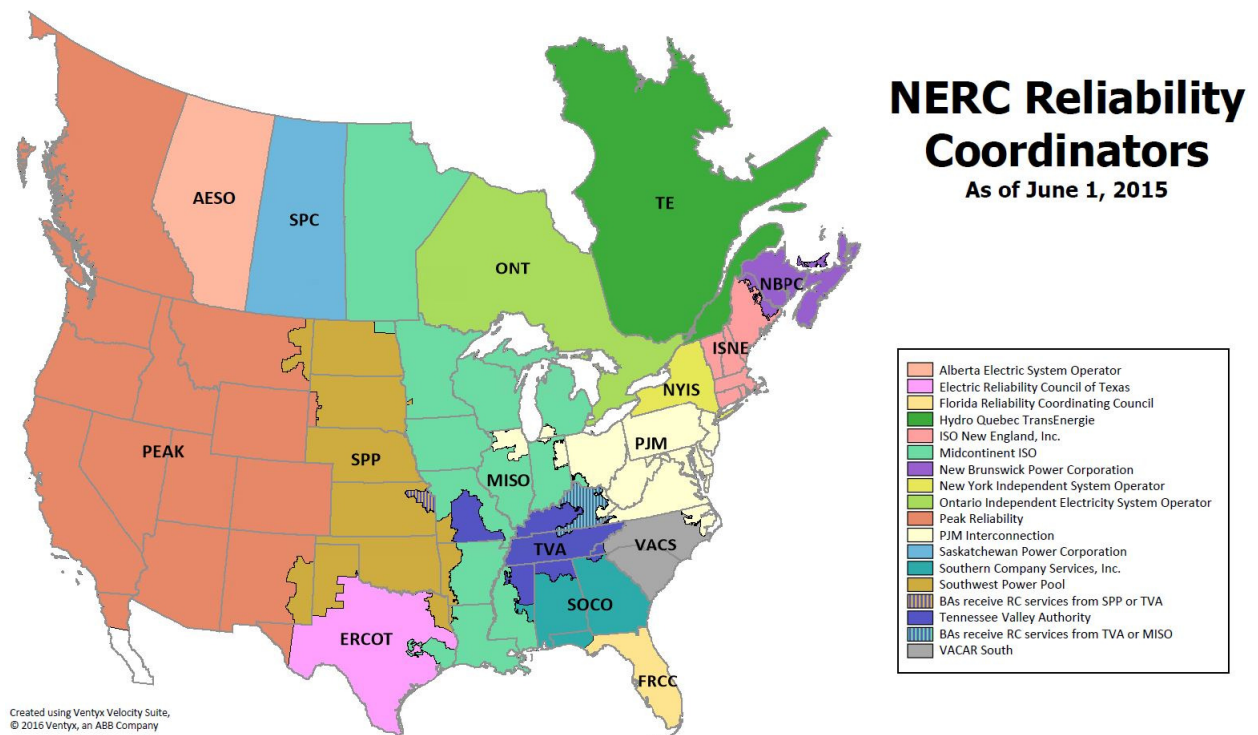


Figure 1.5: Independent system operators in the US.

convergence is conditioned on proper initialization [12]. Reference [13] leverages the theory of monotone operators to tackle GF by solving a set of variational inequalities; while [14] finds GF solutions as the rank-one minimizers of a semi-definite program with a carefully designed cost.

Related to GF are the problems of optimal compression and optimal gas flow (OGF). Optimal compression, which is the task of finding compressor settings with minimal cost while maintaining gas pressures within limits, has been posed as a geometric program in [5]. The OGF task minimizes the costs of procuring gas while respecting pipeline network limitations. Using successive linearization of the involved nonlinear functions, reference [15] tackles OGF

by solving a sequence of convex problems. The problem of minimizing fuel cost consumption due to compressors is discussed in [16]. All the compressors in the network are ignored, resulting in a disconnected network. Each disconnected network is termed as a subnetwork, and the gas flow equations are solved independently for every subnetwork. All the subnetworks are then connected via compressors to form a supernetwork. The flow rate and inlet/outlet pressure of compressors are assumed to be independent of each other, which is not true. Also the proposed model fails to solve GF equations if the supernetwork is mesh.

It has been shown in [15] that for a network without any compressors, the flows and pressures are the optimal primal-dual solution of a convex minimization problem. For general meshed networks with compressors, the GF problem is typically solved using the Newton-Raphson scheme, but its convergence is conditioned on proper initialization [12]. Under slow time-varying injections, the Newton-Raphson scheme could be initialized at the previous state; nevertheless, this may not be applicable for reliability studies. Leveraging the theory of monotone operators [17], preprint [13] shows that a GF solution can be found by solving a set of variational inequalities. The latter are derived from the GF equations after applying a carefully designed linear transformation. The approach is proved successful for tree networks. Otherwise, a quasi-convex optimization problem should be solved to design the linear transformation under the restricting assumptions that flow directions are known a priori.

For modeling the natural gas system, steady-state approximation is widely adopted [18]. A quantitative model that evaluates the effect of fuel uncertainty of natural gas power plants is considered in [19]. The coupling between gas and power networks only appears in terms

of the incurred generation cost also termed as social welfare. The proposed task maximizes the social welfare subject to power flow constraints.

A transient model for coupled natural gas and electricity networks is discussed in [20]. The gas network consumption is modeled as two components: forecasted and small spatio-temporally varying. Furthermore, the pressure fluctuations introduced by time-varying gas demands are discussed. Coordinated scheduling of coupled natural gas and power systems is studied in [8]. The gas flow equations are discretized in space giving rise to a set of ordinary differential equations (ODEs), while the electric system is modeled through the linearized DC power flow model. The formulated optimization problem is non-convex with respect to the continuous-time spaces, and is approximated through non-linear programming. While the optimality is not guaranteed, provable exactness is non-trivial. Reference [21] considers the joint optimization of residential gas distribution networks and radial electric power grids coupled through gas-fired generators. The optimal power flow task relies on the second-order cone (SOC) relaxation of the branch-flow equations [22], whereas the optimal gas flow is handled through the convex-concave approach reviewed in [23] to yield SOC constraints as well. The two systems are computationally decoupled upon using the alternating direction method of multipliers (ADMM); see e.g., [24]. The proposed formulation uses a dynamic model for gas flow equations as described in [25].

# Chapter 2

## Background

This chapter reviews some mathematical tools and algorithms that will be used in later chapters.

### 2.1 Semi-definite programming

Consider a minimization problem as follows:

$$\begin{aligned} \min_{\mathbf{X} \succeq \mathbf{0} \in \mathbb{R}^{N \times N}} \quad & \text{Tr}(\mathbf{X}) \\ \text{s.to} \quad & \text{Tr}(\mathbf{A}_k \mathbf{X}) \leq 0 \end{aligned} \tag{2.1}$$

where matrices  $\{\mathbf{A}_k\}_{k=1}^K$  are of appropriate dimensions.

Problem (2.1) minimizes a linear function with respect to linear matrix inequality and linear inequalities, and is known as a semidefinite program (SDP). Since the problem objective and

constraints are convex, a SDP is a convex optimization problem. Semidefinite programs of up to a few hundreds of variables and/or constraints can be efficiently handled by primal-dual interior point methods [26], [27].

## 2.2 Feasible point pursuit

Non-convex QCQPs have traditionally been tackled using the techniques of semi-definite relaxation or successive convex approximation (SCA); see [28], [23], and references therein. Because the former technique entails solving semidefinite programs, its computational complexity may not scale favorably. Moreover, if the relaxation is not exact, it may not be obvious how to obtain a feasible point.

On the other hand, the SCA technique solves a sequence of convex restrictions of the original non-convex problem [23]. To review SCA particularly for QCQPs, consider the program:

$$\min_{\mathbf{x}} \boldsymbol{\lambda}^\top \mathbf{x} \tag{2.2a}$$

$$\text{s.to } f_m(\mathbf{x}) \leq c_m, \quad m = 1, \dots, M \tag{2.2b}$$

where  $f_m(\mathbf{x}) := \mathbf{x}^\top \mathbf{A}_m \mathbf{x} + \mathbf{b}_m^\top \mathbf{x}$  for  $m = 1, \dots, M$ . Unless  $\mathbf{A}_m \succeq \mathbf{0}$  for all  $m$  or  $M \leq 2$ , problem (2.2) is non-convex and hard to solve in general [28]. Every matrix can be expressed as the sum of a positive semidefinite and a negative semidefinite matrix as  $\mathbf{A}_m = \mathbf{A}_m^+ + \mathbf{A}_m^-$  with  $\mathbf{A}_m^+ \succeq \mathbf{0}$  and  $\mathbf{A}_m^- \preceq \mathbf{0}$ . The SCA method substitutes the constraints in (2.3b) as follows:

$$\mathbf{x}^{k+1} := \arg \min_{\mathbf{x}} \boldsymbol{\lambda}^\top \mathbf{x} \quad (2.3a)$$

$$\text{s.to } \tilde{f}_m(\mathbf{x}, \mathbf{x}^k) \leq c_m, \quad m = 1, \dots, M \quad (2.3b)$$

where  $\tilde{f}_m(\mathbf{x}, \mathbf{z}) := \mathbf{x}^\top \mathbf{A}_m^+ \mathbf{x} + 2\mathbf{z}^\top \mathbf{A}_m^- \mathbf{x} - \mathbf{z}^\top \mathbf{A}_m^- \mathbf{z} + \mathbf{b}_m^\top \mathbf{x}$ , and iterates over  $k$  until convergence. It is not hard to verify that  $f_m(\mathbf{x}) \leq \tilde{f}_m(\mathbf{x}, \mathbf{z})$  for all  $\mathbf{x}$  and  $\mathbf{z}$ , while  $f_m(\mathbf{x}) = \tilde{f}_m(\mathbf{x}, \mathbf{x})$ . Therefore, problem (2.3) constitutes a restriction of the QCQP in (2.2). With the caveat of being initialized at a *feasible*  $\mathbf{x}^0$ , the SCA iterates  $\{\mathbf{x}^k\}$  are guaranteed to yield decreasing costs and converge to a stationary point of (2.2).

To remedy the need for a feasible initial point, (FPP) relaxes the restrictions during the SCA iterates by adding a slack variable  $\delta_m$  in the right-hand side (RHS) of each constraint  $m$  and then penalizing the objective by their sum as [29]

$$(\mathbf{x}^{k+1}, \boldsymbol{\delta}^{k+1}) := \arg \min_{\mathbf{x}, \boldsymbol{\delta}} \boldsymbol{\lambda}^\top \mathbf{x} + \kappa \boldsymbol{\delta}^\top \mathbf{1} \quad (2.4)$$

$$\text{s.to } \tilde{f}_m(\mathbf{x}, \mathbf{x}^k) \leq c_m + \delta_m, \quad \forall m$$

for some large  $\kappa > 0$ . The FPP iterates can be initialized at a random point  $\mathbf{x}^0$ . Note that the time taken by the FPP algorithm to converge depends upon the initial point selection.

## 2.3 Alternating direction method of multipliers

The alternating direction method of multipliers (ADMM) is used to decouple large-scale convex optimization tasks into smaller subproblem that are typically easier to solve. It enjoys

---

**Algorithm 1** Feasible point pursuit (FPP) algorithm
 

---

- 1: **Initialization:** Set  $k = 0$  and randomly initialize the point  $\mathbf{z}$ .
  - 2: Solve the convex QCQP in (2.4).
  - 3: Let  $\mathbf{x}^{k*}$  be the optimal solution at the end of  $k$ -th iteration. Set  $\mathbf{z}^{k+1} = \mathbf{x}^{k*}$ .
  - 4: Set  $k = k + 1$  **till convergence.**
- 

the good convergence properties of the method of multipliers and decoupling of variables from dual decomposition [27].

In its general form, ADMM applied to the optimization problem

$$\min \quad f(\mathbf{x}) + g(\mathbf{y}) \quad (2.5a)$$

$$\text{over } \mathbf{x} \in \mathcal{X}, \mathbf{y} \in \mathcal{Y} \quad (2.5b)$$

$$\text{s.to } \mathbf{x} = \mathbf{y} \quad (2.5c)$$

Let  $\boldsymbol{\lambda}$  be the Lagrange multiplier corresponding to the equality constraint in (2.5c). Given that  $\mathcal{X}$  and  $\mathcal{Y}$  are convex sets, the minimizers  $\mathbf{x}^*$  and  $\mathbf{y}^*$  are found through following iterations:

$$\mathbf{x}^{k+1} \in \arg \min_{\mathbf{x} \in \mathcal{X}} f(\mathbf{x}) + \frac{\rho}{2} \|\mathbf{x} - \mathbf{y}^k + \boldsymbol{\lambda}^k\|_2^2, \quad (2.6a)$$

$$\mathbf{y}^{k+1} \in \arg \min_{\mathbf{y} \in \mathcal{Y}} g(\mathbf{y}) + \frac{\rho}{2} \|\mathbf{x}^{k+1} - \mathbf{y} + \boldsymbol{\lambda}^k\|_2^2, \quad (2.6b)$$

$$\boldsymbol{\lambda}^{k+1} := \boldsymbol{\lambda}^k + (\mathbf{x}^{k+1} - \mathbf{y}^{k+1}), \quad (2.6c)$$

where  $\rho$  is a positive constant. Assuming that  $f$  and  $g$  are convex, the convergence of ADMM

to an optimal solution is guaranteed under following conditions [24]:

$$\lim_{k \rightarrow \infty} \|\mathbf{x}^k - \mathbf{y}^k\|_2 = 0,$$
$$\lim_{k \rightarrow \infty} \|\mathbf{y}^k - \mathbf{y}^{k-1}\|_2 = 0.$$

The method has been adopted in a wide range of applications [30], [31], [32], including optimal power flow and power system state estimation [33], [34], [35].

# Chapter 3

## Steady-state gas flow

### 3.1 Introduction

The increasing variability in gas demand both across time and space calls for advanced modeling, control, and monitoring of the underlying physical infrastructure. In this context, this chapter targets solving efficiently the *gas flow (GF)* equations, a set of nonlinear equations governing the distribution of gas flows and pressures across a pipeline network. Given gas injections and withdrawals across all nodes, the *gas flow* problem aims at finding gas flows across pipelines together with the pressure at all nodes. Even under steady-state and balanced conditions, solving the GF problem is hard to solve for non-tree networks [13].

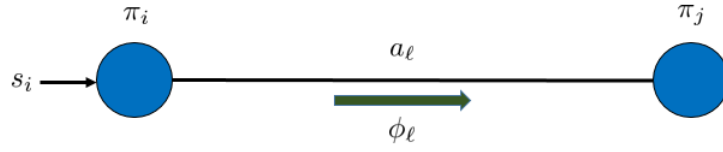
In this chapter, after reviewing a natural gas network model via a convenient matrix-vector notation in Section 3.2, it is first recognized that the GF task can be tackled using a semidef-

inite program (SDP) relaxation in Section 3.3. The relaxation is shown to be exact for a judiciously selected cost of the related SDP problem. Secondly, efficient formulations for designing this cost function and for solving the GF problem are developed in Section 3.4. Numerical tests conducted on a modified version of a part of the Belgian gas network demonstrate: (i) the success of the relaxation over a wide range of injection conditions; and (ii) its superiority over the currently used Newton-Raphson scheme. Conclusions are presented in Section 3.7.

Regarding *notation*, lower- (upper-) case boldface letters denote column vectors (matrices), while symbol  $(\cdot)^\top$  stands for transposition. Calligraphic symbols are reserved for sets, and  $|\mathcal{X}|$  is the cardinality of set  $\mathcal{X}$ . Vectors  $\mathbf{0}$ ,  $\mathbf{1}$ , and  $\mathbf{e}_n$ , are the all-zeros, all-ones, and the  $n$ -th canonical vectors, respectively. Operator  $\text{dg}(\mathbf{x})$  defines a diagonal matrix having  $\mathbf{x}$  on its main diagonal. A symmetric positive (semi)definite matrix is denoted by  $\mathbf{X} \succ \mathbf{0}$  ( $\mathbf{X} \succeq \mathbf{0}$ ). Finally, symbols  $\mathbb{S}^N$  and  $\mathbb{S}_+^N$  ( $\mathbb{S}_{++}^N$ ) denote respectively the sets of  $N \times N$  symmetric and symmetric positive (semi)definite matrices.

## 3.2 Natural gas network modeling

Consider a natural gas network modeled by a directed graph  $\mathcal{G} := (\mathcal{N}_0, \mathcal{L})$ . The graph vertices  $\mathcal{N}_0 = \{0, \dots, N\}$  model nodes where gas is injected or withdrawn from the network, or simple junctions. The graph edges  $\mathcal{L} = \{1, \dots, L\}$  correspond to gas pipelines connecting two network nodes. Let  $\pi_i > 0$  be the gas pressure at node  $i$  for all  $i \in \mathcal{N}_0$ . One of the

Figure 3.1: Gas network pipeline  $(i, j)$ .

nodes (conventionally one hosting a large gas producer) is selected as the reference node, it is indexed by 0, and its gas pressure is fixed to a known value  $\pi_0$ . The remaining nodes form the set  $\mathcal{N} := \{1, \dots, N\}$ . The gas injection  $s_i$  at node  $i \in \mathcal{N}_0$  is positive for an injection node, negative for a withdrawal node, and zero for network junctions. Without loss of generality, edges are assigned an arbitrary direction denoted by  $\ell : (i, j) \in \mathcal{L}$  for  $i, j \in \mathcal{N}_0$ . The gas flow  $\phi_\ell$  on pipeline  $\ell : (i, j) \in \mathcal{L}$  is positive when gas flows from node  $i$  to node  $j$ , and negative, otherwise. Conservation of mass implies that

$$s_i = \sum_{\ell: (i,j) \in \mathcal{L}} \phi_\ell - \sum_{\ell: (j,i) \in \mathcal{L}} \phi_\ell \quad (3.1)$$

for every  $i \in \mathcal{N}_0$ . Moreover, summing injections over all nodes should yield zero in steady state, that is  $s_0 = -\sum_{i \in \mathcal{N}} s_i$ . Therefore, given balanced  $\{s_i\}_{i \in \mathcal{N}_0}$ , model (3.1) provides  $N$  rather than  $N + 1$  independent linear equations on  $\{\phi_\ell\}_{\ell \in \mathcal{L}}$ .

Natural gas networks are operated at high pressures of 200 to 1,500 pounds per square inch (psi), flows amount to millions of cubic feet, and pipelines have diameters in the range of 16–48 inches [5], [36]. Under these conditions, the pressure drop and energy loss over pipelines are captured by a partial differential equation involving one spatial dimension along the pipeline length and the time dimension; see [37] and [38] for details. After ignoring friction, any

possible pipeline tilt, and assuming time-invariant gas injections, for a given pipeline  $(i, j)$  as shown in Fig 3.1, the partial differential equation simplifies to the *Weymouth equation* [5]:

$$\pi_i^2 - \pi_j^2 = a_\ell \phi_\ell |\phi_\ell| \quad (3.2)$$

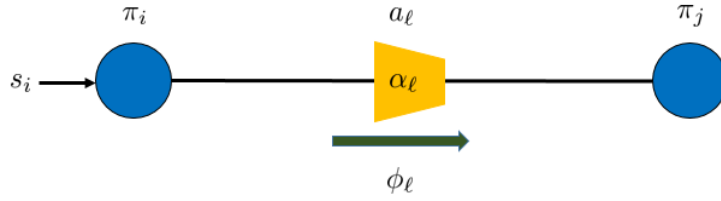
characterizing the pressure difference across the endpoints of pipeline  $\ell : (i, j) \in \mathcal{L}$ . The parameter  $a_\ell > 0$  in (3.2) depends on physical properties of the pipeline, such as its length and diameter [13]. The Weymouth equation asserts that gas pressure drops across a pipeline in the direction of gas flow. To be precise, the difference of squared pressures is proportional to the squared gas flow.

Reliable network operation requires that gas pressures remain within specific limits. To avoid unacceptably low or high pressures, network operators install compressors at selected pipelines, henceforth referred to as *active pipelines* comprising the set  $\mathcal{L}_a \subseteq \mathcal{L}$  with  $L_a = |\mathcal{L}_a|$ . A compressor amplifies the squared pressure between its input and output by a compression ratio  $\alpha_\ell$ . Suppose  $\phi_\ell > 0$  and that the compressor along pipeline  $\ell : (i, j) \in \mathcal{L}_a$  is located at normalized distances  $r_\ell$  with  $r_\ell \in [0, 1]$  from node  $i$  and  $(1 - r_\ell)$  from node  $j$ . It is easy to verify from (3.2) that the pressure at the compressor input is  $\pi_i^2 - r_\ell a_\ell \phi_\ell^2$ , while the pressure at its output is  $\pi_j^2 + (1 - r_\ell) a_\ell \phi_\ell^2$ . The compression ratio is defined as [5]

$$\alpha_\ell := \frac{\pi_j^2 + (1 - r_\ell) a_\ell \phi_\ell^2}{\pi_i^2 - r_\ell a_\ell \phi_\ell^2} \geq 1. \quad (3.3)$$

Since  $\phi_\ell$  is known to be positive for active pipelines, equation (3.3) can be rearranged as

$$\alpha_\ell \pi_i^2 - \pi_j^2 = c_\ell \phi_\ell |\phi_\ell| \quad (3.4)$$

Figure 3.2: Gas network pipeline  $(i, j)$  with compressor.

where  $c_\ell := a_\ell[1 - (1 - \alpha_\ell)r_\ell]$  is a known positive constant. The pressure drop described by (3.4) generalizes the Weymouth equation in (3.2), since it applies to both active and non-active pipelines: one can simply set  $r_\ell = 0$  and  $\alpha_\ell = 1$  for non-active pipelines  $\ell \notin \mathcal{L}_a$ .

Given the reference pressure  $\pi_0$ , balanced nodal injections  $\{s_i\}_{i \in \mathcal{N}_0}$ , and the pipeline parameters  $\{\alpha_\ell, c_\ell\}_{\ell \in \mathcal{L}}$ , the *gas flow (GF) problem* aims at finding nodal pressures  $\{\pi_i\}_{i \in \mathcal{N}}$  and pipeline flows  $\{\phi_\ell\}_{\ell \in \mathcal{L}}$  satisfying the gas flow equations (3.1), (3.4), and  $\{\phi_\ell \geq 0\}_{\ell \in \mathcal{L}_a}$ . It therefore consists of solving  $N + L$  equations over  $N + L$  unknowns. Although equations (3.1) are linear, the generalized Weymouth equation in (3.4) is piecewise quadratic and not everywhere differentiable, while the requirement  $\{\phi_\ell \geq 0\}_{\ell \in \mathcal{L}_a}$  further complicates the task. The GF problem is typically solved using Newton-Raphson iterates [12]. However, the method converges only if it is initialized sufficiently close to the actual system state.

To handle the non-differentiability of the absolute value in (3.4), introduce variable  $\psi_\ell = |\phi_\ell|$  for all  $\ell \in \mathcal{L}$ ; see also [13]. The latter equation can be equivalently written as  $\psi_\ell^2 = \phi_\ell^2$  and  $\psi_\ell \geq 0$  for all  $\ell$ . To express the gas flow equations in a matrix-vector form, stack all edge quantities in vectors  $\boldsymbol{\phi} := [\phi_1 \ \cdots \ \phi_L]^\top$ ,  $\boldsymbol{\psi} := [\psi_1 \ \cdots \ \psi_L]^\top$ ,  $\mathbf{c} := [c_1 \ \cdots \ c_L]^\top$ , and  $\boldsymbol{\alpha} := [\alpha_1 \ \cdots \ \alpha_L]^\top$ . Excluding the reference bus, collect also nodal quantities in  $\boldsymbol{\pi} := [\pi_1 \ \cdots \ \pi_N]^\top$

and  $\mathbf{s} := [s_1 \cdots s_N]^\top$ .

The connectivity of the gas network graph is captured by the  $L \times (N + 1)$  incidence matrix

$\tilde{\mathbf{A}}$  with entries

$$\tilde{A}_{\ell,n} = \begin{cases} +1, & n = i \\ -1, & n = j \\ 0, & \text{otherwise} \end{cases} \quad \forall \ell : (i, j) \in \mathcal{L}. \quad (3.5)$$

Isolating the first column corresponding to the reference node, matrix  $\tilde{\mathbf{A}}$  can be partitioned as

$\tilde{\mathbf{A}} = [\mathbf{a}_0 \ \mathbf{A}]$ . Having introduced the reduced incidence matrix  $\mathbf{A}$ , equation (3.1) is equivalent

to  $s_0 = \mathbf{a}_0^\top \boldsymbol{\phi}$  and  $\mathbf{s} = \mathbf{A}^\top \boldsymbol{\phi}$ . Because  $\tilde{\mathbf{A}}\mathbf{1} = \mathbf{0}$ , equation  $s_0 = \mathbf{a}_0^\top \boldsymbol{\phi}$  can be ignored assuming

balanced steady-state injections satisfying  $s_0 = -\mathbf{1}^\top \mathbf{s}$ . The gas flow problem can now be

compactly expressed as [13]

$$\mathbf{A}^\top \boldsymbol{\phi} = \mathbf{s} \quad (3.6a)$$

$$\mathbf{B}(\boldsymbol{\pi} \odot \boldsymbol{\pi}) = \mathbf{c} \odot \boldsymbol{\phi} \odot \boldsymbol{\psi} - p_0^2 \mathbf{b}_0 \quad (3.6b)$$

$$\boldsymbol{\phi} \odot \boldsymbol{\phi} = \boldsymbol{\psi} \odot \boldsymbol{\psi} \quad (3.6c)$$

$$\boldsymbol{\psi} \geq \mathbf{0} \quad (3.6d)$$

$$\phi_l \geq 0, \quad \forall l \in \mathcal{L}_a \quad (3.6e)$$

where  $\odot$  denotes the Hadamard (entry-wise) product. Matrix  $\mathbf{B}$  and vector  $\mathbf{b}_0$  are defined

as [13]

$$\mathbf{B} := \text{dg}(\boldsymbol{\alpha})[\mathbf{A}]_+ - [-\mathbf{A}]_+ \quad (3.7a)$$

$$\mathbf{b}_0 := \text{dg}(\boldsymbol{\alpha})[\mathbf{a}_0]_+ - [-\mathbf{a}_0]_+ \quad (3.7b)$$

where the positive part operator  $[x]_+ := \max\{0, x\}$  is applied entrywise for vectors and matrices.

If the gas network is a tree, then  $L = N$  and matrices  $\mathbf{A}$  and  $\mathbf{B}$  are square and invertible. In this case, the vector of gas flows  $\boldsymbol{\phi}$  can be readily found from (3.6a) and the vector of nodal pressures  $\boldsymbol{\pi}$  can be subsequently calculated through (3.6b). In practice though, natural gas networks exhibit a non-radial structure [3].

For a gas network without compressors, matrix  $\text{dg}(\boldsymbol{\alpha})$  becomes the identity matrix  $\mathbf{I}_L$  and thus  $\mathbf{B} = \mathbf{A}$  and  $\mathbf{b}_0 = \mathbf{a}_0$ . Under this setup, pipeline flows can be found as the minimizers of the convex optimization problem [15]

$$\min_{\boldsymbol{\phi}} \sum_{\ell=1}^L \frac{a_{\ell}}{3} |\phi_{\ell}|^3 \quad (3.8a)$$

$$\text{s.to } \mathbf{A}^{\top} \boldsymbol{\phi} = \mathbf{s}. \quad (3.8b)$$

Moreover, the related nodal pressures  $\mathbf{p}$  can be recovered through the  $(N + 1)$ -length vector  $\boldsymbol{\xi}$  of the optimal Lagrange multipliers corresponding to (3.8b). In detail, vector  $\boldsymbol{\xi}$  can be shifted by a constant without loss of optimality. If this constant is selected such that the first entry of  $\boldsymbol{\xi}$  is  $p_0^2$ , the remaining entries of  $\boldsymbol{\xi}$  are equal to the squared nodal pressures. This approach fails in the presence of compressors, for which case the scheme described next could be followed.

### 3.3 Semidefinite program relaxation (SDR)

Based on the previous modeling, the gas flow problem entails finding the  $2N + L$  unknowns  $(\boldsymbol{\phi}, \boldsymbol{\psi}, \boldsymbol{\pi})$  through the  $N$  linear equations of (3.6a) and the  $2L$  quadratic equations of (3.6b)–(3.6c) under the  $L + L_a$  linear inequalities of (3.6d)–(3.6e). Since the system involves quadratic equations, it is hard to solve in general. Nevertheless, computational tasks pertaining to quadratic (in)equalities have been successfully tackled using the powerful tool of semidefinite programming (SDP) relaxations with applications in various fields including clustering in data mining [39]; beamforming and symbol detection in wireless communications [28]; power system operation tasks [40], [41]; and phase retrieval in signal processing [42]; to name a few. Spurred by these results, the gas flow problem is tackled next as an SDP.

The GF problem involves non-homogeneous quadratic functions of the unknowns since the linear functions of (3.6a) are coupled with the homogeneous quadratic functions in (3.6d)–(3.6e). To convert all functions to homogeneous quadratic ones [28], let us augment the unknown variables as  $\mathbf{x} := [\boldsymbol{\phi}^\top \ \boldsymbol{\psi}^\top \ \boldsymbol{\pi}^\top \ 1]^\top$  having length  $K := 2L + N + 1$ . The vector  $\mathbf{x}$  will be also referred to as the *system state vector*. Each equation in (3.6a)–(3.6c) is expressible as a homogeneous quadratic equality constraint on  $\mathbf{x}$  as

$$\mathbf{x}^\top \mathbf{M}_k \mathbf{x} = s_k \tag{3.9}$$

where  $\mathbf{M}_k \in \mathbb{S}^K$  and  $s_k \in \mathbb{R}$  for  $k = 1, \dots, K - 1$ . In detail, if equality  $k$  in (3.9) corresponds to:

(a) the  $i$ -th linear equality in (3.6a), then  $s_k := q_i$  and

$$\mathbf{M}_k := \frac{1}{2} \begin{bmatrix} \mathbf{0} & \mathbf{0} & \mathbf{0} & \mathbf{a}_i \\ \mathbf{0} & \mathbf{0} & \mathbf{0} & \mathbf{0} \\ \mathbf{0} & \mathbf{0} & \mathbf{0} & \mathbf{0} \\ \mathbf{a}_i^\top & \mathbf{0}^\top & \mathbf{0}^\top & 0 \end{bmatrix}$$

where  $\mathbf{a}_i$  is the  $i$ -th column of  $\mathbf{A}$ ;

(b) the  $\ell$ -th entry of (3.6b), then  $s_k := -p_0^2 b_{0,\ell}$  and

$$\mathbf{M}_k := \frac{1}{2} \begin{bmatrix} \mathbf{0} & -c_\ell \text{dg}(\mathbf{e}_\ell) & \mathbf{0} & \mathbf{0} \\ -c_\ell \text{dg}(\mathbf{e}_\ell) & \mathbf{0} & \mathbf{0} & \mathbf{0} \\ \mathbf{0} & \mathbf{0} & 2 \text{dg}(\mathbf{b}_\ell) & \mathbf{0} \\ \mathbf{0}^\top & \mathbf{0}^\top & \mathbf{0}^\top & 0 \end{bmatrix}$$

where  $\mathbf{b}_\ell$  is the  $\ell$ -th row of  $\mathbf{B}$ ;

(c) the  $\ell$ -th entry of (3.6c), then  $s_k := 0$  and

$$\mathbf{M}_k := \frac{1}{2} \begin{bmatrix} \text{dg}(\mathbf{e}_\ell) & \mathbf{0} & \mathbf{0} & \mathbf{0} \\ \mathbf{0} & -\text{dg}(\mathbf{e}_\ell) & \mathbf{0} & \mathbf{0} \\ \mathbf{0} & \mathbf{0} & \mathbf{0} & \mathbf{0} \\ \mathbf{0}^\top & \mathbf{0}^\top & \mathbf{0}^\top & 0 \end{bmatrix}.$$

(d) To guarantee that the last entry of  $\mathbf{x}$  is unity, introduce the additional constraint  $x_K^2 = 1$ .

The latter can also be posed as in (3.9) by selecting  $s_K := 1$  and  $\mathbf{M}_K := \mathbf{e}_K \mathbf{e}_K^\top$ . If  $x_K$  turns out to be  $-1$ , then vector  $-\mathbf{x}$  is a GF solution in lieu of  $\mathbf{x}$ .

Likewise, the linear inequalities in (3.6d)–(3.6e) are written as

$$\mathbf{x}^\top \mathbf{N}_m \mathbf{x} \leq 0 \quad (3.10)$$

for  $\mathbf{N}_m \in \mathbb{S}^K$ . If inequality  $\ell$  in (3.10) corresponds to:

(a) the  $\ell$ -th inequality in (3.6d), then

$$\mathbf{N}_m := \frac{1}{2} \begin{bmatrix} \mathbf{0} & \mathbf{0} & \mathbf{0} & \mathbf{0} \\ \mathbf{0} & \mathbf{0} & \mathbf{0} & -\mathbf{e}_\ell \\ \mathbf{0} & \mathbf{0} & \mathbf{0} & \mathbf{0} \\ \mathbf{0}^\top & -\mathbf{e}_\ell^\top & \mathbf{0}^\top & 0 \end{bmatrix}; \text{ or}$$

(b) the  $\ell$ -th inequality of (3.6e), then

$$\mathbf{N}_m := \frac{1}{2} \begin{bmatrix} \mathbf{0} & \mathbf{0} & \mathbf{0} & -\mathbf{e}_\ell \\ \mathbf{0} & \mathbf{0} & \mathbf{0} & \mathbf{0} \\ \mathbf{0} & \mathbf{0} & \mathbf{0} & \mathbf{0} \\ -\mathbf{e}_\ell^\top & \mathbf{0}^\top & \mathbf{0} & 0 \end{bmatrix}.$$

Solving (3.6) can be now expressed as the feasibility problem:

$$\begin{aligned} & \text{find } \mathbf{x} & (3.11) \\ & \text{s.to } \mathbf{x}^\top \mathbf{M}_k \mathbf{x} = d_k, \quad k = 1, \dots, K \\ & \mathbf{x}^\top \mathbf{N}_m \mathbf{x} \leq 0, \quad m = 1, \dots, L + L_a. \end{aligned}$$

Nonetheless, solving (3.11) remains computationally hard because the problem involves quadratic (in)equalities as well. To tackle the non-convexity, we leverage the technique

of semidefinite program relaxation (SDR) [28]. To that end, introduce the matrix variable  $\mathbf{X} \in \mathbb{S}^K$  and upon enforcing  $\mathbf{X} = \mathbf{x}\mathbf{x}^\top$ , rewrite problem (3.11) equivalently as

$$\begin{aligned} & \underset{\mathbf{X}=\mathbf{x}\mathbf{x}^\top}{\text{find}} && (\mathbf{X}, \mathbf{x}) && (3.12) \\ & \text{s.to} && \text{Tr}(\mathbf{M}_k \mathbf{X}) = d_k, \quad k = 1, \dots, K \\ & && \text{Tr}(\mathbf{N}_m \mathbf{X}) \leq 0, \quad m = 1, \dots, L + L_a. \end{aligned}$$

The constraint  $\mathbf{X} = \mathbf{x}\mathbf{x}^\top$  can be equivalently expressed as  $\mathbf{X} \succeq \mathbf{0}$  and  $\text{rank}(\mathbf{X}) = 1$ . By introducing these two constraints in (3.12), the original variable  $\mathbf{x}$  can be eliminated. Moreover, the resultant feasibility problem can be transformed to a minimization problem by assigning the objective  $\text{Tr}(\mathbf{M}\mathbf{X})$  for some  $\mathbf{M} \in \mathbb{S}_+^K$ :

$$\begin{aligned} & \underset{\mathbf{X} \succeq \mathbf{0}}{\min} && \text{Tr}(\mathbf{M}\mathbf{X}) && (3.13) \\ & \text{s.to} && \text{Tr}(\mathbf{M}_k \mathbf{X}) = d_k, \quad k = 1, \dots, K \\ & && \text{Tr}(\mathbf{N}_m \mathbf{X}) \leq 0, \quad m = 1, \dots, L + L_a \\ & && \text{rank}(\mathbf{X}) = 1. \end{aligned}$$

Enforcing the rank constraint in (3.13) though is NP hard in general [28]. The SDR technique suggests relaxing the feasible set of (3.13) by dropping its rank constraint to get:

$$\underset{\mathbf{X} \succeq \mathbf{0}}{\min} \text{Tr}(\mathbf{M}\mathbf{X}) \tag{3.14a}$$

$$\text{s.to} \quad \text{Tr}(\mathbf{M}_k \mathbf{X}) = d_k, \quad k = 1, \dots, K \tag{3.14b}$$

$$\text{Tr}(\mathbf{N}_m \mathbf{X}) \leq 0, \quad m = 1, \dots, L + L_a \tag{3.14c}$$

that is a convex SDP problem. Due to the relaxation, the optimal value of (3.14) serves as a lower bound on the optimal value of (3.13). Moreover, if the minimizer  $\hat{\mathbf{X}}$  of (3.14) turns out to be rank-1, then  $\hat{\mathbf{X}}$  is feasible for the problem in (3.13) as well, the optimal values in (3.13) and (3.14) coincide, and therefore  $\hat{\mathbf{X}}$  is a minimizer of the non-convex SDP in (3.13). In this case, the relaxation is deemed *exact*, and the sought solution  $\hat{\mathbf{x}}$  to (3.12) is obtained by simply decomposing  $\hat{\mathbf{X}}$  as  $\hat{\mathbf{X}} = \hat{\mathbf{x}}\hat{\mathbf{x}}^\top$ .

The existence of a rank-1 solution for (3.14) depends on the network parameters along with the specification vector  $\mathbf{d} := [d_1 \ \cdots \ d_K]^\top$ . On the other hand, the matrix  $\mathbf{M} \in \mathbb{S}_+^K$  appearing in the objective of (3.14) offers multiple degrees of freedom. Inspired by an approach followed to obtain solutions to the power flow problem via a relaxed SDP [43], [44], the next section selects  $\mathbf{M}$  to favor a rank-1 minimizer of (3.14).

### 3.4 Objective function design

To design matrix  $\mathbf{M}$ , consider the mapping  $\mathbf{s}(\mathbf{x}) : \mathbb{R}^K \rightarrow \mathbb{R}^K$  whose  $k$ -th entry is  $s_k(\mathbf{x}) := \mathbf{x}^\top \mathbf{M}_k \mathbf{x}$  for  $k = 1, \dots, K$ . The associated Jacobian matrix evaluated at  $\mathbf{x}$  is

$$\mathbf{J}(\mathbf{x}) = 2[\mathbf{M}_1 \mathbf{x} \ \dots \ \mathbf{M}_K \mathbf{x}]. \quad (3.15)$$

Since the mapping  $\mathbf{s}(\mathbf{x})$  is continuous, the inverse function theorem asserts that  $\mathbf{s}(\mathbf{x})$  is invertible close to  $\mathbf{x}$  if  $\mathbf{J}(\mathbf{x})$  is invertible. By the definition of  $\mathbf{s}(\mathbf{x})$ , the Jacobian matrix  $\mathbf{J}(\mathbf{x})$  is sparse for all  $\mathbf{x}$ . However, the invertibility of  $\mathbf{J}(\mathbf{x})$  depends on  $\mathbf{x}$ , and it thus hard to characterize. For this reason, we resort to studying the generic rank of  $\mathbf{J}(\mathbf{x})$ , which is the

maximal rank over all possible values for the non-zero entries of  $\mathbf{J}(\mathbf{x})$ .

**Proposition 1.** *The Jacobian matrix  $\mathbf{J}(\mathbf{x})$  associated with the mapping  $\mathbf{s}(\mathbf{x})$  is full rank in general.*

*Proof of Prop. 1.* The generic rank of  $\mathbf{J}(\mathbf{x})$  is characterized using a result from [45]. Specifically, given a matrix  $\mathbf{C} \in \mathbb{R}^{N \times N}$ , construct a graph with  $2N$  nodes. Nodes  $\{v_i\}_{i=1}^N$  correspond to the rows of  $\mathbf{C}$  and nodes  $\{u_j\}_{j=1}^N$  correspond to its columns. An edge is drawn between nodes  $v_i$  and  $u_j$  only if  $C_{ij} \neq 0$ . If each node  $u_j$  can be matched to a different node  $v_i$ , then  $\mathbf{C}$  is full rank in general.

To apply the previous result, it is not hard to verify that the sparsity pattern of  $\mathbf{J}(\mathbf{x})$  is captured by the binary matrix

$$\mathbf{J}_b = \begin{bmatrix} |\mathbf{A}| & \mathbf{I}_L & \mathbf{I}_L & \mathbf{0} \\ \mathbf{0} & \mathbf{I}_L & \mathbf{I}_L & \mathbf{0} \\ \mathbf{0} & |\mathbf{A}|^\top & \mathbf{0} & \mathbf{0} \\ \mathbf{0}^\top & \mathbf{0}^\top & \mathbf{0}^\top & 1 \end{bmatrix}$$

where  $|\mathbf{A}|$  is the matrix with the absolute values of  $\mathbf{A}$ . The last column of  $\mathbf{J}_b$  can be matched to its last row due to the entry 1. Moreover, its third block column can be matched to its second block row due to  $\mathbf{I}_L$ . The remaining entries of  $\mathbf{J}_b$  form the matrix

$$\tilde{\mathbf{J}}_b = \begin{bmatrix} |\mathbf{A}| & \mathbf{I}_L \\ \mathbf{0} & |\mathbf{A}|^\top \end{bmatrix}.$$

Consider a spanning tree on the graph  $\mathcal{G}$  representing the gas network. Without loss of generality, pipelines can be renumbered so that  $\mathbf{A}$  is partitioned as  $\mathbf{A} = [\mathbf{A}_s^\top \ \mathbf{A}_n^\top]^\top$ , where

the  $N \times N$  submatrix  $\mathbf{A}_s$  corresponds to the pipelines comprising the spanning tree, and the  $(L - N) \times N$  submatrix  $\mathbf{A}_n$  to the remaining pipelines. Matrix  $\tilde{\mathbf{J}}_b$  can be then partitioned as

$$\tilde{\mathbf{J}}_b = \begin{bmatrix} |\mathbf{A}_s| & \mathbf{I}_N & \mathbf{0} \\ |\mathbf{A}_n| & \mathbf{0} & \mathbf{I}_{L-N} \\ \mathbf{0} & |\mathbf{A}_s|^\top & |\mathbf{A}_n|^\top \end{bmatrix}.$$

The third block column of  $\tilde{\mathbf{J}}_b$  can be matched to its second block row due to  $\mathbf{I}_{L-N}$  and the remaining submatrix is

$$\hat{\mathbf{J}}_b = \begin{bmatrix} |\mathbf{A}_s| & \mathbf{I}_N \\ \mathbf{0} & |\mathbf{A}_s|^\top \end{bmatrix}.$$

Heed that each column of  $|\mathbf{A}_s|$  corresponds to a node in  $\mathcal{G}$  excluding node 0. Since every such node can be the destination end of a pipeline in the spanning tree, every column of  $|\mathbf{A}_s|$  is guaranteed to have an 1 entry at a different row. Hence, the first column block of  $\hat{\mathbf{J}}_b$  is matched to its first row block. By the same argument, the second block row of  $\hat{\mathbf{J}}_b$  is matched to its second block column. A perfect matching has thus been found between the columns and rows of  $\mathbf{J}(\mathbf{x})$ .  $\square$

Proposition 1, guarantees only the generic invertibility of  $\mathbf{J}(\mathbf{x})$ . Nevertheless, all the Jacobian matrices evaluated during the numerical tests of Section 3.6 were invertible.

Let us next derive the dual problem of the relaxed SDP in (3.14). To this end, let  $\boldsymbol{\lambda} \in \mathbb{R}^K$  and  $\boldsymbol{\mu} \in \mathbb{R}^{2L}$  be the Lagrange multipliers corresponding to (3.14b) and (3.14c), respectively.

The dual problem of (3.14) is the SDP

$$\begin{aligned} \max_{\lambda, \mu \geq \mathbf{0}} \quad & -\boldsymbol{\lambda}^\top \mathbf{d} \\ \text{s.to} \quad & \mathbf{M} + \sum_{k=1}^K \lambda_k \mathbf{M}_k + \sum_{m=1}^{2L} \mu_m \mathbf{N}_m \succeq \mathbf{0}. \end{aligned} \quad (3.16)$$

To simplify the presentation, define the matrix

$$\mathbf{Z}(\boldsymbol{\lambda}, \boldsymbol{\mu}) := \mathbf{M} + \sum_{k=1}^K \lambda_k \mathbf{M}_k + \sum_{m=1}^{2L} \mu_m \mathbf{N}_m. \quad (3.17)$$

In addition, let function  $h_2(\mathbf{Z})$  be the sum of the two smallest eigenvalues of  $\mathbf{Z}$ , which is known to be concave over  $\mathbb{S}_+^K$  [27].

Adopting the approach in [43], the next result provides sufficient conditions for  $\mathbf{M}$  to yield an exact gas flow relaxation for a specific state vector  $\hat{\mathbf{x}}$ .

**Proposition 2.** *Consider a gas network state  $\hat{\mathbf{x}}$  with specifications  $\hat{\mathbf{s}} := \mathbf{s}(\hat{\mathbf{x}})$  and invertible Jacobian matrix  $\mathbf{J}(\hat{\mathbf{x}})$ . If there exists a vector  $\hat{\boldsymbol{\lambda}}$  such that:*

- (c1)  $\mathbf{M}\hat{\mathbf{x}} + \frac{1}{2}\mathbf{J}(\hat{\mathbf{x}})\hat{\boldsymbol{\lambda}} = \mathbf{0}$ ;
- (c2)  $\hat{\mathbf{Z}} := \mathbf{Z}(\hat{\boldsymbol{\lambda}}, \mathbf{0}) \succeq \mathbf{0}$ ; and
- (c3)  $h_2(\hat{\mathbf{Z}}) \geq \epsilon$  for an  $\epsilon > 0$ ;

then  $\hat{\mathbf{X}} := \hat{\mathbf{x}}\hat{\mathbf{x}}^\top$  is the unique minimizer of (3.13) for specifications  $\hat{\mathbf{s}}$ .

*Proof of Proposition 2.* The objective in (3.14) is bounded below by zero. Assuming there exists feasible matrix  $\mathbf{X} \succ \mathbf{0}$ , strong duality holds between (3.14) and its dual problem in (3.16), and the Karush-Kuhn-Tucker (KKT) conditions apply [46, Lemma 1].

By (c2), matrix  $\hat{\mathbf{Z}}$  is dual feasible. It further holds that:

$$\hat{\mathbf{Z}}\hat{\mathbf{x}} = \mathbf{M}\hat{\mathbf{x}} + \sum_{k=1}^K \lambda_k \mathbf{M}_k \hat{\mathbf{x}} = \mathbf{M}\hat{\mathbf{x}} + \mathbf{J}(\hat{\mathbf{x}})\hat{\boldsymbol{\lambda}} = \mathbf{0}$$

where the second equality follows from the definition of the Jacobian matrix in (3.15), and the third one from condition (c1). Then, it holds that  $\hat{\mathbf{Z}}\hat{\mathbf{X}} = \hat{\mathbf{Z}}\hat{\mathbf{x}}\hat{\mathbf{x}}^\top = \mathbf{0}$ . Because the  $\{\hat{\mu}_m\}_{m=1}^{2L}$  corresponding to  $\hat{\boldsymbol{\lambda}}$  and  $\hat{\mathbf{Z}}$  have been set to zero,  $\mu_m \text{Tr}(\mathbf{N}_m \hat{\mathbf{X}}) = 0$  holds for all  $m$ . Therefore,  $\hat{\mathbf{X}}$  and  $\hat{\mathbf{Z}}$  satisfy the complementary slackness conditions.

Since  $\hat{\mathbf{X}}$  and  $\hat{\mathbf{Z}}$  satisfy the KKT conditions, they are primal and dual optimal. This proves that  $\hat{\mathbf{x}}$  is a minimizer of (3.14); its uniqueness is addressed next.

Because  $\hat{\mathbf{Z}}\hat{\mathbf{x}} = \mathbf{0}$  and  $\hat{\mathbf{Z}} \succeq \mathbf{0}$ , the smallest eigenvalue of  $\hat{\mathbf{Z}}$  is zero. From (c3), the second smallest eigenvalue of  $\hat{\mathbf{Z}}$  is strictly positive, and therefore  $\text{rank}(\hat{\mathbf{Z}}) = K - 1$ . Complementary slackness asserts that every minimizer  $\tilde{\mathbf{X}}$  of (3.14) satisfies  $\hat{\mathbf{Z}}\tilde{\mathbf{X}} = \mathbf{0}$ . The latter implies that  $\text{rank}(\tilde{\mathbf{X}}) \leq 1$ ; see [46]. Since  $\tilde{\mathbf{X}} = \mathbf{0}$  is not feasible, all minimizers of (3.14) have to be rank one, i.e., they are of the form  $\tilde{\mathbf{X}} = \tilde{\mathbf{x}}\tilde{\mathbf{x}}^\top$  for some  $\tilde{\mathbf{x}}$  with  $\mathbf{d}(\tilde{\mathbf{x}}) = \hat{\mathbf{d}}$ . The invertibility of  $\mathbf{J}(\hat{\mathbf{x}})$  guarantees that the mapping  $\mathbf{d}(\hat{\mathbf{x}})$  is locally invertible, and hence, there is no  $\tilde{\mathbf{x}}$  with  $\tilde{\mathbf{x}} \neq \hat{\mathbf{x}}$  matching the specifications  $\hat{\mathbf{s}}$ . The latter proves the uniqueness of  $\hat{\mathbf{x}}$  and concludes the proof.  $\square$

Proposition 2 asserts that if  $\mathbf{M}$  satisfies (c1)–(c3), then the relaxation in (3.14) is exact for a given system state  $\hat{\mathbf{x}}$  with invertible Jacobian matrix  $\mathbf{J}(\hat{\mathbf{x}})$ . This fact may seem to be of limited interest, since it guarantees the success of SDR only for this particular  $\hat{\mathbf{x}}$ . Nevertheless, the continuity argument adopted in [43, Th. 2] on the exactness of SDR for

the power flow problem applies here too. Therefore, it follows that the relaxation in (3.14) is exact for all realizable states  $\mathbf{x}$  with an invertible Jacobian matrix lying in a ball around  $\hat{\mathbf{x}}$ .

To design matrix  $\mathbf{M}$  such that the SDR is exact over a wider range of system states, conditions (c1)–(c3) can be enforced for multiple system states of interest  $\mathbf{x}_i$  for  $i = 1, \dots, R$ . These states could reflect representative flow patterns in the natural gas network and could be selected based on the experience of the gas network operator. The task of finding  $\mathbf{M}$  satisfying the conditions of Prop. 2 for  $\{\mathbf{x}_i\}_{i=1}^R$  can be posed as the feasibility problem [43]

$$\text{find } (\mathbf{M}, \{\boldsymbol{\lambda}_i\}) \quad (3.18a)$$

$$\text{s.to } \mathbf{M}\mathbf{x}_i + \frac{1}{2}\mathbf{J}(\mathbf{x}_i)\boldsymbol{\lambda}_i = \mathbf{0}, \quad \forall i \quad (3.18b)$$

$$\mathbf{Z}(\boldsymbol{\lambda}_i, \mathbf{0}) \succeq \mathbf{0}, \quad \forall i \quad (3.18c)$$

$$h_2(\mathbf{Z}(\boldsymbol{\lambda}_i, \mathbf{0})) \geq \epsilon, \quad \forall i \quad (3.18d)$$

where  $\epsilon > 0$ . Given that function  $h_2(\mathbf{Z})$  is concave over  $\mathbb{S}_+^K$ , the feasibility problem in (3.18) is convex. In fact, it can be converted to an SDP minimization by (i) appending a linear objective over  $\mathbf{M}$  such as  $\text{Tr}(\mathbf{M})$ ; and (ii) converting the constraints in (3.18d) into a set of SDP constraints.

The key point in converting (3.18d) is that the sum of the two smallest eigenvalues of a positive semidefinite matrix  $\mathbf{Z}$  admits the SDP characterization [47, pp. 67–68]:

$$h_2(\mathbf{Z}) = \max_{\mathbf{W}, \gamma} -\text{Tr}(\mathbf{W}) - 2\gamma \quad (3.19a)$$

$$\text{s.to } \mathbf{Z} + \gamma\mathbf{I} + \mathbf{W} \succeq \mathbf{0} \quad (3.19b)$$

$$\mathbf{W} \succeq \mathbf{0}. \quad (3.19c)$$

Expressing  $h_2(\mathbf{Z})$  as in (3.19) implies that if there exist  $(\mathbf{W}, \gamma)$  satisfying (3.19b)–(3.19c) and also  $\text{Tr}(\mathbf{W}) + 2\gamma + \epsilon \leq 0$ , then  $h_2(\mathbf{Z}) \geq -\text{Tr}(\mathbf{W}) - 2\gamma \geq \epsilon$ .

Designing  $\mathbf{M}$  can be now posed as the SDP:

$$\text{find } (\mathbf{M}, \{\mathbf{W}_i, \boldsymbol{\lambda}_i, \gamma_i\}_{i=1}^R) \quad (3.20a)$$

$$\text{s.to } \mathbf{M}\mathbf{x}_i + \frac{1}{2}\mathbf{J}(\mathbf{x}_i)\boldsymbol{\lambda}_i = \mathbf{0}, \quad \forall i \quad (3.20b)$$

$$\mathbf{M} + \sum_{k=1}^K \lambda_{i,k}\mathbf{M}_k \succeq \mathbf{0}, \quad \forall i \quad (3.20c)$$

$$\text{Tr}(\mathbf{W}_i) + 2\gamma_i + \epsilon \leq 0, \quad \forall i \quad (3.20d)$$

$$\mathbf{M} + \sum_{k=1}^K \lambda_i(k)\mathbf{M}_k + \gamma_i\mathbf{I} + \mathbf{W}_i \succeq \mathbf{0}, \quad \forall i \quad (3.20e)$$

$$\mathbf{W}_i \succeq \mathbf{0}, \quad \forall i \quad (3.20f)$$

where  $\lambda_{i,k}$  is the  $k$ -th entry of variable  $\boldsymbol{\lambda}_i$ . Note that in transitioning from (3.18) to (3.20), each matrix  $\mathbf{Z}(\boldsymbol{\lambda}_i, \mathbf{0})$  has been substituted by its definition in (3.17). Moreover, the constraint in (3.18d) has been transformed to constraints (3.20d)–(3.20f).

Adding more points while designing  $\mathbf{M}$  could yield a better coverage of the operating conditions of the gas network. On the other hand, adding more test points  $\{\mathbf{x}_i\}$  increases the computational complexity of the problem in (3.20). It should be underlined however that the task of designing  $\mathbf{M}$  is performed once, whereas solving the GF equations via (3.14) is executed in real-time multiple times per day.

### 3.5 An alternative approach

By introducing the matrix variable  $\mathbf{X} = \mathbf{x}\mathbf{x}^\top$  in Section 3.3, we were able to construct all monomials of first and second degree involving the variables  $\{\phi_\ell, \psi_\ell\}_\ell$  and  $\{p_n\}_n$ . However, the gas flow equations in (3.6) involve only the products  $\{\phi_\ell^2, \psi_\ell^2, \phi_\ell\psi_\ell\}_\ell$  and  $\{p_n^2\}_n$ . Building on this observation, an alternative SDR solver for the gas flow task is devised next.

Since nodal pressures appear only squared in (3.6), define the variable  $\boldsymbol{\beta}$  with entries  $\beta_n = p_n^2$  for all  $n \in \mathcal{N}$ . For every line  $\ell \in \mathcal{L}$ , define  $\mathbf{x}_\ell := [\phi_\ell \ \psi_\ell \ 1]^\top$  and introduce the constraint  $\mathbf{X}_\ell = \mathbf{x}_\ell\mathbf{x}_\ell^\top$ . Similar to Section 3.3, the gas flow problem can be formulated as the SDP:

$$\min_{\{\mathbf{x}_\ell \succeq \mathbf{0}\}, \boldsymbol{\beta} \succeq \mathbf{0}} \sum_{\ell \in \mathcal{L}} \text{Tr}(\mathbf{M}^\ell \mathbf{X}_\ell) + \mathbf{g}^\top \boldsymbol{\beta} \quad (3.21a)$$

$$\text{s.to} \quad \sum_{\ell \in \mathcal{L}} A_{\ell,i} \text{Tr}(\bar{\mathbf{M}}_1 \mathbf{X}_\ell) = s_i \quad \forall i \in \mathcal{N} \quad (3.21b)$$

$$c_\ell \text{Tr}(\bar{\mathbf{M}}_2 \mathbf{X}_\ell) = \mathbf{b}_\ell^\top \boldsymbol{\beta} + p_0^2 b_{0,\ell} \quad \forall \ell \in \mathcal{L} \quad (3.21c)$$

$$\text{Tr}(\bar{\mathbf{M}}_3 \mathbf{X}_\ell) = 0 \quad \forall \ell \in \mathcal{L} \quad (3.21d)$$

$$\text{Tr}(\bar{\mathbf{M}}_4 \mathbf{X}_\ell) = 1 \quad \forall \ell \in \mathcal{L} \quad (3.21e)$$

$$\text{Tr}(\bar{\mathbf{N}}_1 \mathbf{X}_\ell) \leq 0 \quad \forall \ell \in \mathcal{L} \quad (3.21f)$$

$$\text{Tr}(\bar{\mathbf{N}}_2 \mathbf{X}_\ell) \leq 0 \quad \forall \ell \in \mathcal{L}_a \quad (3.21g)$$

where  $A_{\ell,i}$  is the  $(\ell, i)$ -th entry of  $\mathbf{A}$  and  $\mathbf{b}_\ell^\top$  is the  $\ell$ -th row of  $\mathbf{B}$ . The matrices appearing in (3.21) are defined as:

$$\bar{\mathbf{M}}_1 := \frac{1}{2}(\mathbf{e}_1\mathbf{e}_3^\top + \mathbf{e}_3\mathbf{e}_1^\top)$$

$$\bar{\mathbf{M}}_2 := \frac{1}{2}(\mathbf{e}_1\mathbf{e}_2^\top + \mathbf{e}_2\mathbf{e}_1^\top)$$

$$\begin{aligned}\bar{\mathbf{M}}_3 &:= \frac{1}{2}(\mathbf{e}_1\mathbf{e}_1^\top - \mathbf{e}_2\mathbf{e}_2^\top) & \bar{\mathbf{M}}_4 &:= \frac{1}{2}\mathbf{e}_3\mathbf{e}_3^\top \\ \bar{\mathbf{N}}_1 &:= -\frac{1}{2}(\mathbf{e}_2\mathbf{e}_3^\top + \mathbf{e}_3\mathbf{e}_2^\top) & \bar{\mathbf{N}}_2 &:= -\frac{1}{2}(\mathbf{e}_1\mathbf{e}_3^\top + \mathbf{e}_3\mathbf{e}_1^\top)\end{aligned}$$

where  $\mathbf{e}_1$ ,  $\mathbf{e}_2$ , and  $\mathbf{e}_3$  are the canonical vectors in  $\mathbb{R}^3$ . Since  $\boldsymbol{\beta}$  is not part of any  $\mathbf{X}_\ell$ , its inner product with a vector  $\mathbf{d}$  has been added in the cost. The SDR solver of (3.21) is successful if all the minimizing  $\{\mathbf{X}_\ell\}$  are rank-1. The parameters  $\{\mathbf{M}^\ell\}$  and  $\mathbf{g}$  are designed next to promote such rank-one minimizers.

Let  $(\bar{\boldsymbol{\lambda}}, \bar{\boldsymbol{\delta}}, \bar{\boldsymbol{\mu}}, \bar{\boldsymbol{\gamma}}, \bar{\boldsymbol{\theta}}, \bar{\boldsymbol{\nu}})$  be the Lagrange multipliers associated with constraints (3.21b)–(3.21g), respectively. The dual problem of (3.21) can be written as:

$$\begin{aligned}\max \quad & -\bar{\boldsymbol{\lambda}}^\top \mathbf{s} - \pi_0^2 \bar{\boldsymbol{\delta}}^\top \mathbf{b}_0 - \bar{\boldsymbol{\gamma}}^\top \mathbf{1} \\ \text{over} \quad & \bar{\boldsymbol{\lambda}}, \bar{\boldsymbol{\delta}}, \bar{\boldsymbol{\mu}}, \bar{\boldsymbol{\gamma}}, \bar{\boldsymbol{\theta}} \succeq \mathbf{0}, \bar{\boldsymbol{\nu}} \succeq \mathbf{0} \\ \text{s.to} \quad & \mathbf{Z}_\ell(\bar{\boldsymbol{\lambda}}, \bar{\boldsymbol{\delta}}, \bar{\boldsymbol{\mu}}, \bar{\boldsymbol{\gamma}}, \bar{\boldsymbol{\theta}}, \bar{\boldsymbol{\nu}}) \succeq \mathbf{0} \quad \forall \ell \\ & \mathbf{g} - \mathbf{B}^\top \bar{\boldsymbol{\delta}} = \mathbf{0}\end{aligned}$$

where  $\mathbf{Z}_\ell(\bar{\boldsymbol{\lambda}}, \bar{\boldsymbol{\delta}}, \bar{\boldsymbol{\mu}}, \bar{\boldsymbol{\gamma}}, \bar{\boldsymbol{\theta}}, \bar{\boldsymbol{\nu}}) := \mathbf{M}^\ell + \sum_{i=1}^N \bar{\lambda}_i A_{\ell,i} \bar{\mathbf{M}}_1 + \bar{\delta}_\ell c_\ell \bar{\mathbf{M}}_2 + \bar{\mu}_\ell \bar{\mathbf{M}}_3 + \bar{\gamma}_\ell \bar{\mathbf{M}}_4 + \bar{\theta}_\ell \bar{\mathbf{N}}_1 + \bar{\nu}_\ell \bar{\mathbf{N}}_2$ .

Extending the results of Proposition 2, it can be verified that if there exist vectors  $\bar{\boldsymbol{\lambda}}^*$ ,  $\bar{\boldsymbol{\delta}}^*$ ,  $\bar{\boldsymbol{\mu}}^*$  and  $\bar{\boldsymbol{\gamma}}^*$  such that:

$$(c1^*) \hat{\mathbf{Z}}_\ell := \mathbf{Z}_\ell(\bar{\boldsymbol{\lambda}}^*, \bar{\boldsymbol{\delta}}^*, \bar{\boldsymbol{\mu}}^*, \bar{\boldsymbol{\gamma}}^*, \mathbf{0}, \mathbf{0}) \succeq \mathbf{0} \quad \forall \ell;$$

$$(c2^*) \hat{\mathbf{Z}}_\ell \hat{\mathbf{x}}_\ell = \mathbf{0} \quad \forall \ell;$$

$$(c3^*) h_2(\hat{\mathbf{Z}}_\ell) \geq \epsilon \text{ for an } \epsilon > 0 \quad \forall \ell; \text{ and}$$

$$(c4^*) \hat{\boldsymbol{\beta}} \odot (\mathbf{g} - \mathbf{B}^\top \bar{\boldsymbol{\delta}}^*) = \mathbf{0};$$

then  $\hat{\mathbf{X}}_\ell = \hat{\mathbf{x}}_\ell \hat{\mathbf{x}}_\ell^\top$  for all  $\ell \in \mathcal{L}$  and  $\hat{\boldsymbol{\beta}}$  are the unique minimizers of (3.21) for input specifications  $(p_0, \mathbf{q})$ . Assuming a realistic scenario in which  $\hat{\boldsymbol{\beta}} \succ \mathbf{0}$ , (c4\*) can be equivalently expressed as:  $\mathbf{g} - \mathbf{B}^\top \boldsymbol{\delta} = \mathbf{0}$ .

Enforcing conditions (c1\*) – (c4\*) for multiple system states  $\{\mathbf{x}_i\}_{i=1}^R$  leads to the feasibility problem of finding  $\{\mathbf{M}^\ell\}_{\ell \in \mathcal{L}}$  and  $\mathbf{g}$ .

$$\begin{aligned}
& \text{find } \left( \{\mathbf{M}^\ell\}_{\ell=1}^L, \mathbf{g}, \{\bar{\boldsymbol{\lambda}}_i, \bar{\boldsymbol{\delta}}_i, \bar{\boldsymbol{\mu}}_i, \bar{\boldsymbol{\gamma}}_i\}_{i=1}^R \right) & (3.22) \\
& \text{s.to } \mathbf{Z}_\ell^i \succeq \mathbf{0} & \forall \ell, i \\
& \mathbf{Z}_\ell^i \mathbf{x}_\ell^i = \mathbf{0} & \forall \ell, i \\
& h_2(\mathbf{Z}_\ell^i) \geq \epsilon & \forall \ell, i \\
& \mathbf{g} = \mathbf{B}^\top \bar{\boldsymbol{\delta}}_i & \forall i
\end{aligned}$$

where  $\epsilon > 0$ . Using the alternative representation for  $h_2(\mathbf{Z}_\ell^i)$ , problem (3.22) can be expressed and solved as an SDP similar to (3.20).

## 3.6 Numerical tests

The developed SDR approaches for solving the gas flow equations were tested on a benchmark system that is part of the Belgian natural gas network [3], see Fig 3.4 for the entire network. The network contains 20 nodes connected with 19 pipelines, two of which are active ones with compressor ratios equal to 1.5, see Fig. 3.2. Although the original network contains loops, its publicized version has been simplified to a tree. Additional pipelines were added

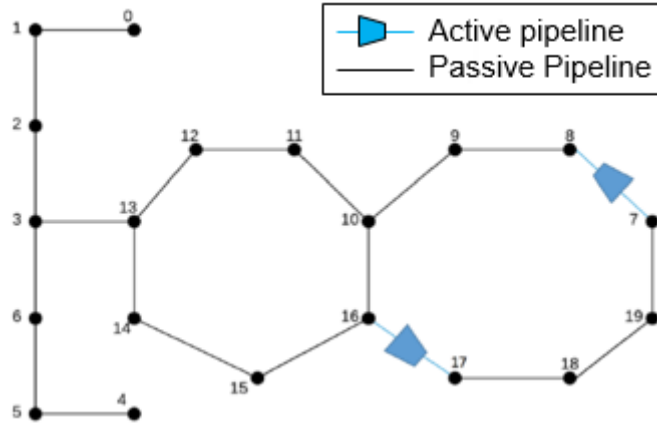


Figure 3.3: Modified Belgian gas network [3].

between nodes 13-16, and 7-19. Pairs of pipelines running in parallel were replaced by a single equivalent pipeline. The characteristics of pipelines are presented in Table 3.1. All SDP problems were solved on a laptop with a 2.7 GHz Intel Core i5 processor with 8GB RAM using the SDPT3 solver in YALMIP [48], [49].

At first, matrix  $\mathbf{M}$  was designed according to the process of Section 3.4 using  $R$  system states  $\{\mathbf{x}_i\}_{i=1}^R$  constructed as follows. A vector of nominal nodal pressures was set to the values shown in the second column of Table 3.2. Given nodal pressures, pipeline flows were found using the Weymouth equation in (3.6b). These nodal pressures and pipeline flows comprised vector  $\mathbf{x}_1$ . Nodal gas injections were calculated from (3.6a) and are shown in the third column of Table 3.2. The nominal pressure vector was subsequently perturbed using a zero-mean Gaussian distribution with standard deviation of 0.25% the nominal pressure to generate  $(R - 1)$  additional pressure vectors  $\{\boldsymbol{\pi}_i\}_{i=2}^R$ . Repeating the previous process for all pressure vectors, a total of  $R$  valid system states  $\{\mathbf{x}_i\}_{i=1}^R$  was obtained. The points were

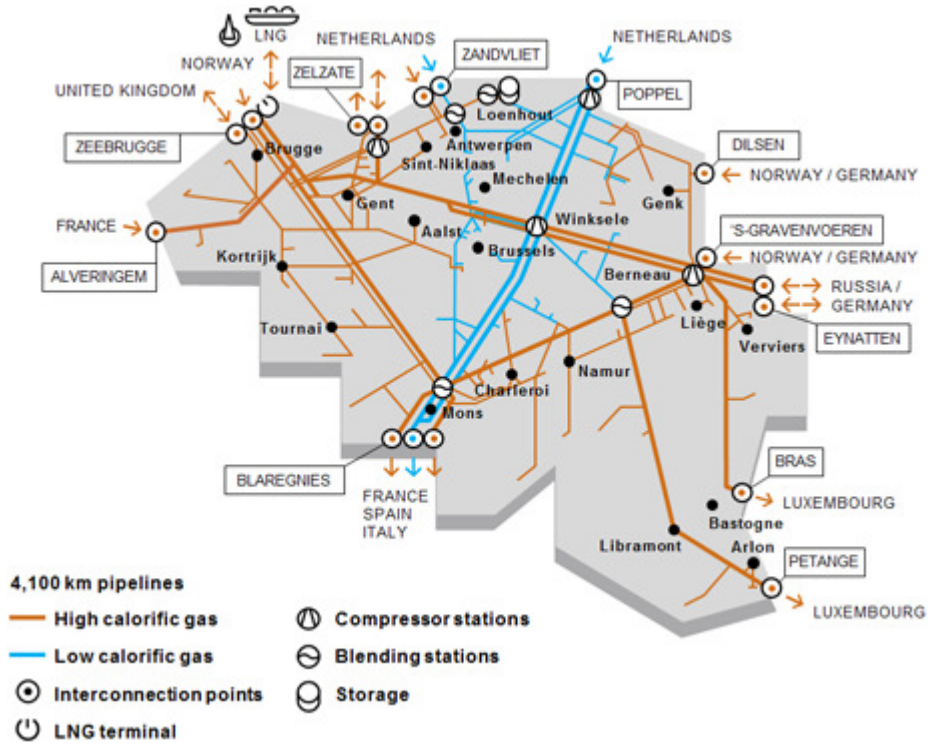


Figure 3.4: Belgian gas network [4].

used to find  $\mathbf{M}$  by solving (3.20) for  $\epsilon = 0.1$ .

Due to the nonlinear nature of the gas flow equations, small variations to nodal pressures result in large variations in gas injections and flows. This is demonstrated in Table 3.2 whose fourth and fifth columns show respectively the perturbations and injections corresponding to  $\mathbf{x}_2$ . Slight perturbations of pressures from  $\mathbf{x}_1$  (second column) to  $\mathbf{x}_2$  (fourth column) yield large variations or even sign reversals in gas injections (third and fifth columns).

Having designed matrix  $\mathbf{M}$ , we then tested the efficacy of the developed SDR gas flow solver over multiple randomly generated gas network states. These validation states were constructed following a process similar to the one described for designing  $\mathbf{M}$ ; yet now per-

Table 3.1: Pipeline Description

From	To	$a_\ell$	From	To	$a_\ell$
0	1	0.0275	10	11	1.157
1	2	0.0413	11	12	1.1025
2	3	0.7166	12	13	0.1378
4	5	9.9745	13	14	0.2756
5	6	6.7270	14	15	0.6981
3	6	4.4073	10	16	19.4384
3	13	1.5159	16	17	155.7688
7	8	0.1095	17	18	587.1301
8	9	0.4379	18	19	35.9467
9	10	0.5473	16	15	1.1025
17	19	1.1025			

turbation was set to  $\zeta 0.25\%$  of the nominal pressure vector with  $\zeta$  ranging from 0 to 1 in increments of 0.05. For each value of  $\zeta$ , 200 system states were generated. States for which gas flows on active pipelines did not agree with the prescribed direction were ignored. An insight on how perturbed pressures affect gas injections is shown in Fig. 3.5.

For every test system state  $\mathbf{x}$ , the related specifications  $\mathbf{d}(\mathbf{x})$  were provided as inputs to the SDR technique. The design process took 317, 776 and 2361 seconds for  $R$  equal to 3, 4, and

5, respectively.

If the SDP optimization in (3.14) yielded a rank-1 minimizer  $\hat{\mathbf{X}}$ , the related  $\hat{\mathbf{x}}$  was calculated via the decomposition  $\hat{\mathbf{X}} = \hat{\mathbf{x}}\hat{\mathbf{x}}^\top$ . If additionally the obtained  $\hat{\mathbf{x}}$  was within a Euclidean distance of  $10^{-6}$  from the actual  $\mathbf{x}$ , the SDR was deemed successful. The same gas flow equations were also solved using the Newton-Raphson iterates initialized at the actual state perturbed by a vector whose entries were drawn uniformly in the range  $\pm 0.025\%$ . The probability of the Newton-Raphson algorithm converging to the actual state, and the probability of successful recovery of the gas flow solution using SDR scheme is plotted against  $\zeta$  in Fig. 3.6. As evidenced by 3.6, the developed SDR scheme operates over a wider range of gas network conditions, while its performance improves for increasing  $R$ .

We subsequently evaluated the alternative SDR scheme of section 3.5. The process of designing  $\{\mathbf{M}^\ell\}_{\ell=1}^L$  took 4, 6, and 8 seconds for  $R$  equal to 8, 16, and 24, respectively. To demonstrate the success of alternative approach for a wide range of gas network conditions, the probability of success was plotted against  $\zeta$  in Fig. 3.7. As evidenced by Fig. 3.7, the alternative SDR scheme has higher probability of success for a wide range of gas network conditions. Finally, note that irrespective of the approach used to design the objective function, the time taken to compute  $\mathbf{x}$  was 5 seconds.

## 3.7 Conclusions

Solving the gas flow equations governing routinely the operation of natural gas networks has been posed as a set of quadratic equalities and inequalities. The latter has been reformulated as a feasibility problem that is also computationally intractable. The problem has been relaxed to a semidefinite program minimization upon dropping the rank constraints. The objective function has been carefully designed so that the relaxation is successful around pre-specified states of possible interest. The advantages of the method over the classic Newton-Raphson approach were demonstrated using a Belgian natural gas network. Spurred by these promising results, our current work focuses on improving the computational complexity of the solver by exploiting the sparse problem structure. Distributed implementations of the technique scalable to networks having thousands of nodes could be pursued. Variations of the gas flow problem with different specification sets such as fixed pressures at some key buses, could be also of interest to gas network operators. The developed computational toolbox is expected to help in understanding and properly modeling the coupling between natural gas and the electric grid infrastructures.

Table 3.2: Nominal &amp; Perturbed Gas Pressures and Injections

Node	Nominal pressures	Nominal injections	Perturbed pressures	Perturbed injections
0	56.5885	14.1383	56.5885	-12.8207
1	56.5395	5.1280	56.6285	30.2602
2	56.4029	-3.9246	56.5173	-0.9886
3	54.8771	0.0007	54.7747	-2.0105
4	53.8119	2.8146	53.9231	2.9580
5	53.0726	-4.0337	53.1077	-2.0875
6	53.1667	-5.2562	53.0597	-7.3482
7	49.5265	22.0105	49.4716	20.3114
8	60.1084	0.0019	60.1225	0.9686
9	58.3168	-6.3653	58.4502	-5.6113
10	57.1563	-0.0002	57.2892	1.0736
11	55.2782	-2.1200	55.1836	-3.9245
12	53.9699	1.1991	54.0969	2.3477
13	53.7673	0.9608	53.8902	2.8507
14	52.4579	-6.8484	52.4541	-8.3078
15	50.8311	-38.8262	50.9074	-38.0651
16	56.2715	23.2105	56.2706	22.5182
17	62.2422	0.0000	62.2179	0.0137
18	34.3912	-0.2220	34.4627	-0.2055
19	32.4096	-1.9190	32.4570	-1.9323

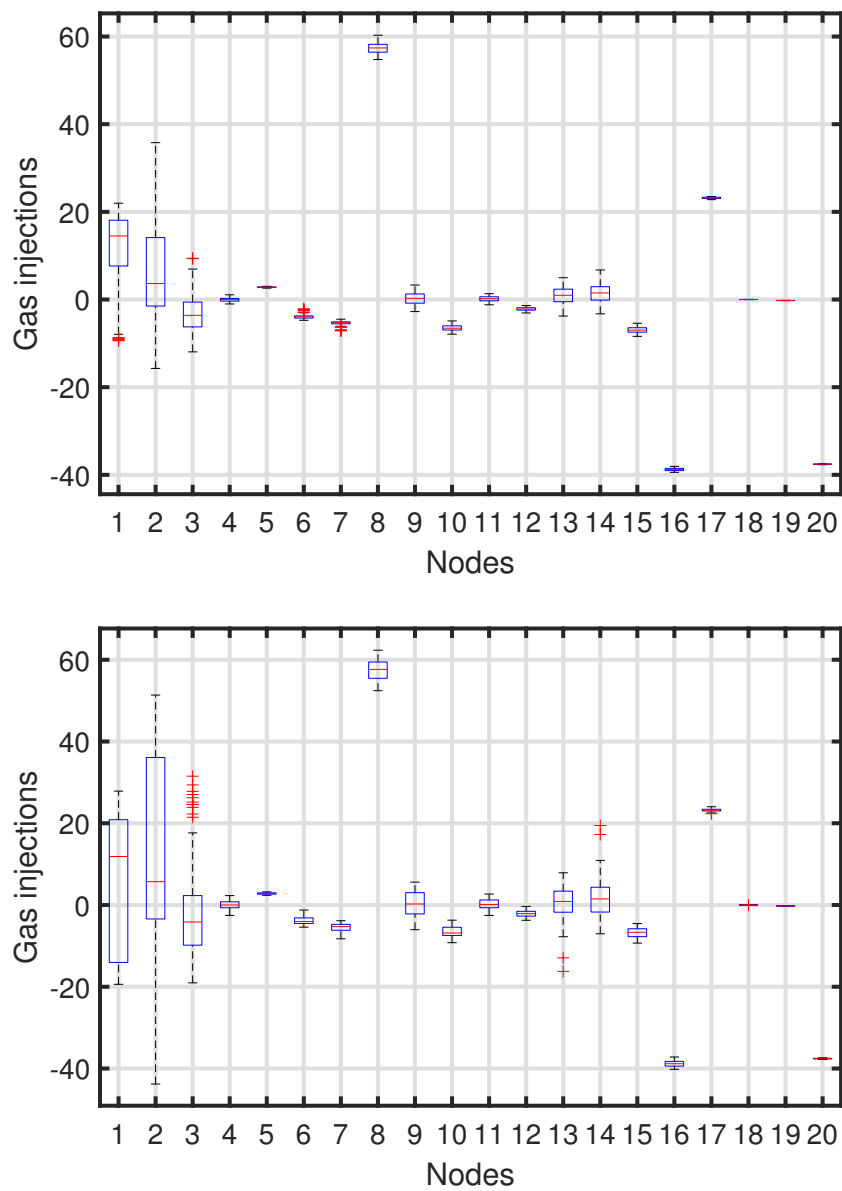


Figure 3.5: Injection variability for perturbing nodal gas pressures by  $\zeta = 0.5$  (top) and  $\zeta = 1.0$  (bottom).

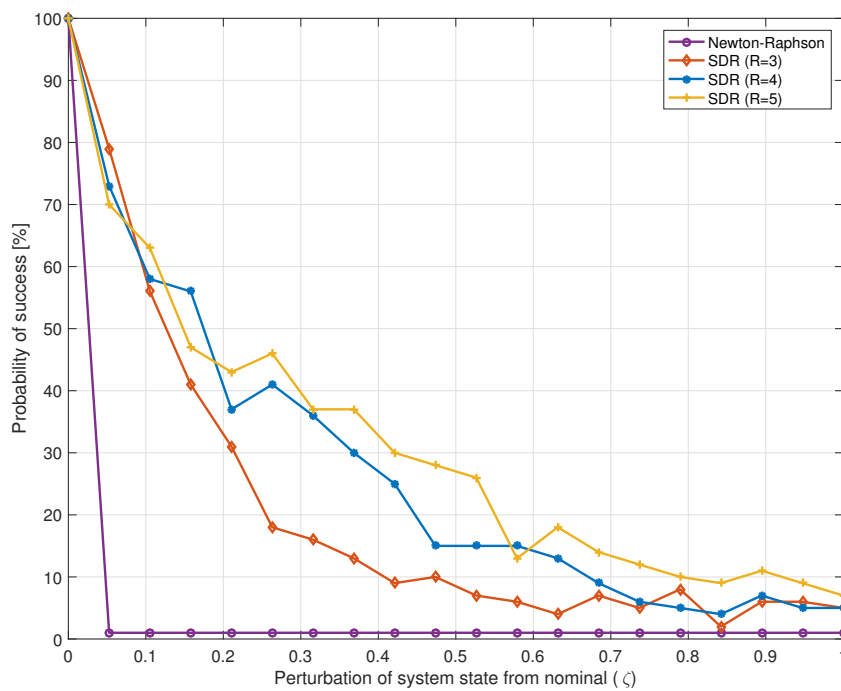


Figure 3.6: Probability of success for Newton-Raphson and the SDR schemes.

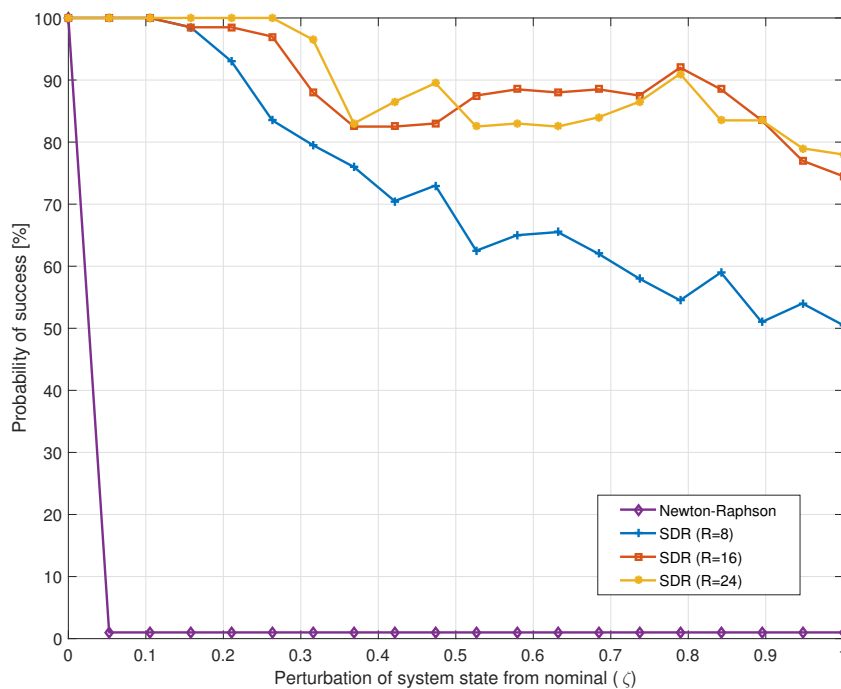


Figure 3.7: Probability of success for the alternative SDR scheme.

# Chapter 4

## Optimal dispatch of coupled electricity and natural gas networks

### 4.1 Introduction

In this chapter, the problem of optimal dispatch of coupled natural gas and electric power systems is tackled. Unlike the previous chapter where gas flow was considered to be steady state, this chapter considers gas flow dynamics. The gas and power systems are coupled through gas-fired generators. For modeling the power system DC power flow equations are considered.

After developing a spatially and temporally discretized dynamic gas and power flow model in Section 4.2, it is first recognized in Section 4.3 that the optimal dispatch task can be

tackled using the feasible point pursuit (FPP) approach of [29]. Secondly, a distributed algorithm using ADMM is developed in Section 4.4 to solve every iteration of FPP. The proposed algorithm has a closed-form solution for select iterative subproblem. Numerical tests conducted on a part of a Belgian gas network coupled with the IEEE 14-bus power network demonstrate the success of distributed algorithm over a wide range of load profiles. Numerical results corroborate enhancements in computationally efficiency over the MINLP approaches and the devised FPP approach . The chapter is concluded in Section 4.6.

## 4.2 Problem statement

In the previous chapter, an algorithm was developed for solving the steady-state gas flow equations. However, the interconnection of gas and power networks introduces dynamics in the natural gas system primarily due to the presence of renewable generation on the power system side. This demands investigating the dynamic model of coupled gas and electric power systems.

After reviewing the physical models governing natural gas networks and electric power systems, this section formulates the problem of their joint dispatch. Natural gas networks are operated at high pressures of 10 to 100 bars, flows amount to millions of cubic feet, and pipelines have diameters in the range of 16–48 inches [5], [36]. Under isothermal conditions, the gas flow in a pipeline is described by the mass conservation and momentum equations [36], [50]. These equations can be simplified upon ignoring terms related to inertia

and kinetic energy, and if the pipeline is assumed to be lying horizontally without tilt. Then, the flow rate  $\phi$  in kg/m<sup>2</sup>s and the pressure  $\pi$  in bars, at time  $t$  and distance  $x$  along a pipeline satisfy the partial differential equations [51]

$$\nu \frac{\partial \pi}{\partial t} + \frac{\partial \phi}{\partial x} = 0 \quad (4.1a)$$

$$\pi \frac{\partial \pi}{\partial x} + \mu \phi |\phi| = 0 \quad (4.1b)$$

where  $\mu$  and  $\nu$  are positive constants determined by the diameter of the pipeline, its friction coefficient, the ambient temperature, and the compressibility of gas. If the gas injection and withdrawal at the endpoints of a pipeline are equal and time-invariant, equation (4.1a) asserts that pressure remains time-invariant as well. Under the same steady-state conditions and by integrating (4.1b) across space, it can be readily shown that the squared pressure across a pipeline drops quadratically with respect to the gas flow, a physical law known as the Weymouth equation [37].

Different from power systems, fluctuations in gas demands can incur spatiotemporal variations in pressures and flows lasting for several hours. To integrate gas dynamics into power system operation, our coupled formulation relies on the dynamic gas flow model in (4.1) that is typically handled through discretization [51], [21]. The time horizon is divided into  $T + 1$  time slots of duration  $\delta_t$  indexed by  $t \in \mathcal{T} := \{0, 1, \dots, T\}$ . Moreover, each pipeline is discretized spatially into segments of length  $\delta_x$  as shown in Fig. 4.1. Consider the pipeline segment  $(i, j)$  running across gas nodes  $i$  and  $j$ . Let  $\phi_{ij}^t$  denote the flow leaving node  $i$ , and  $\phi_{ji}^t$  the flow entering node  $j$  through segment  $(i, j)$  at time  $t$ . Since gas network operators typically know the direction of gas in pipelines [8], the flows  $\phi_{ij}^t$  and  $\phi_{ji}^t$  are assumed positive.

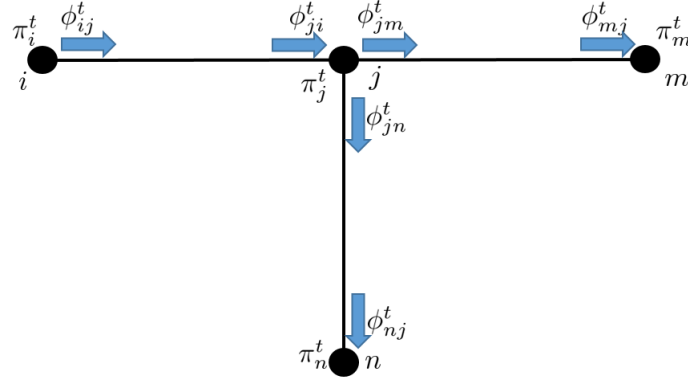


Figure 4.1: Gas network segments.

A gas network node  $i$  may be the endpoint of a pipeline or of a pipeline segment introduced for discretization. Either way, its pressure at time  $t$  is represented by variable  $\pi_i^t$ . Pressures are bounded above due to pipeline limitations and below due to contractual agreements for gas delivery [5]. Thus, the nodal pressures are confined within

$$\underline{\pi}_i \leq \pi_i^t \leq \bar{\pi}_i, \quad \forall t \in \mathcal{T}. \quad (4.2)$$

Adopting the implicit method of finite differences, the gas dynamics in the pipeline segment  $(i, j)$  can be approximated as [51], [21]

$$\tilde{\nu}_{ij}(\pi_i^t + \pi_j^t) = \tilde{\nu}_{ij}(\pi_i^{t-1} + \pi_j^{t-1}) + \phi_{ij}^t - \phi_{ji}^t \quad (4.3a)$$

$$(\pi_i^t)^2 - (\pi_j^t)^2 = \tilde{\mu}_{ij}(\phi_{ij}^t + \phi_{ji}^t)^2 \quad (4.3b)$$

for  $t \in \mathcal{T}$  and where  $\tilde{\mu}_{i,j} := \mu_{ij}/\delta_x$  and  $\tilde{\nu}_{i,j} := \nu_{i,j}/\delta_t$  if  $(\mu_{ij}, \nu_{ij})$  are the constants corresponding to  $(\mu, \nu)$  in (4.1) for this specific pipeline.

The interconnection of an electric power system with a natural gas network is represented by a directed graph  $\mathcal{G} := (\mathcal{N}_0, \mathcal{L})$ . The graph vertices  $\mathcal{N}_0$  model gas injection/withdrawal

nodes; power injection/withdrawal buses; or zero-injection junction nodes. Junction nodes include the intermediate points needed for spatially segmenting pipelines. For simplicity, every network node hosts at most one producer or consumer of gas or power. The vertex subsets  $\mathcal{N}_g$  and  $\mathcal{N}_p$  consist of gas network and the power system nodes, respectively. While  $\mathcal{N}_g \cup \mathcal{N}_p = \mathcal{N}_0$ , system nodes hosting gas-fired generators constituting  $\mathcal{N}_g \cap \mathcal{N}_p$ .

The edge set  $\mathcal{L}$  is partitioned into the subset  $\mathcal{L}_g$  associated with gas pipeline segments and the subset  $\mathcal{L}_p$  associated with transmission lines. Without loss of generality, the edges in  $\mathcal{L}_g$  are oriented in the direction of gas flow, while the edges in  $\mathcal{L}_p$  are assigned an arbitrary direction.

The node in  $\mathcal{N}_g$  hosting the largest gas producer is indexed by  $i = 0$  and its pressure is fixed to a known value  $\pi_0$  [5]. If variable  $\phi_i^t$  captures the gas injection at node  $i \in \mathcal{N}_g$  at time  $t$ , flow conservation implies

$$\phi_i^t = \sum_{(i,j) \in \mathcal{L}_g} \phi_{ij}^t - \sum_{(j,i) \in \mathcal{L}_g} \phi_{ji}^t, \quad \forall i \in \mathcal{N}_g, t \in \mathcal{T}. \quad (4.4)$$

To model gas demands and procurement capacities, gas injections are constrained within known ranges

$$\underline{\phi}_i^t \leq \phi_i^t \leq \overline{\phi}_i^t, \quad \forall t \in \mathcal{T}. \quad (4.5)$$

For the intermediate nodes introduced for spatially discretizing pipelines it holds that  $\underline{\phi}_i^t = \overline{\phi}_i^t = 0$ ; for nodes procuring gas  $\underline{\phi}_i^t \geq 0$ ; and those nodes consuming gas  $\overline{\phi}_i^t \leq 0$  at all  $t \in \mathcal{T}$ .

To guarantee (4.2) despite the pressure drop dictated by (4.3), gas networks are equipped with compressors across specific pipelines. Let  $\mathcal{L}_a \subset \mathcal{L}_g$  be the subset of pipeline segments

with a compressor installed. The compressor on segment  $(i, j) \in \mathcal{L}_a$  amplifies the pressure between its endpoints as [52]

$$\pi_i^t = \alpha_{ij}^t \pi_j^t, \quad \forall t \in \mathcal{T} \quad (4.6)$$

by a given ratio  $\alpha_{ij}^t$ , while the flow rate remains unaltered  $\phi_{ij}^t = \phi_{ji}^t$  at all  $t \in \mathcal{T}$ . Because the cost of operating a compressor depends on  $(\phi_{ij}^t, \alpha_{ij}^t)$  and  $\pi_i^t$ , the ratios  $\alpha_{ij}^t$  are oftentimes optimally selected [53]. Nevertheless, to keep the problem tractable, compression ratios are assumed known here.

Since gas withdrawals are primarily dependent on active power generation, the commonly used linearized DC flow model is adopted for the electric power system; see also [54], [55], [56]. According to this model, the power flow on transmission line  $(i, j) \in \mathcal{L}_p$  with per unit reactance  $x_{ij}$  is approximated by  $(\theta_i^t - \theta_j^t)/x_{ij}$ , where  $\theta_i^t$  is the voltage angle at node  $i \in \mathcal{N}_p$  and time  $t$  expressed in radians. The ensuing constraints guarantee that power flows remain within the transmission line limits  $\bar{p}_{ij}$

$$-\bar{p}_{ij} \leq \frac{\theta_i^t - \theta_j^t}{x_{ij}} \leq \bar{p}_{ij}, \quad \forall (i, j) \in \mathcal{L}_p, t \in \mathcal{T}. \quad (4.7)$$

Analogously to (4.4), if  $p_i^t$  is the active power injection at node  $i \in \mathcal{N}_p$  and time  $t$ , conservation of power implies

$$p_i^t = \sum_{(i,j) \in \mathcal{L}_p} \frac{\theta_i^t - \theta_j^t}{x_{ij}} - \sum_{(j,i) \in \mathcal{L}_p} \frac{\theta_j^t - \theta_i^t}{x_{ji}}, \quad \forall i \in \mathcal{N}_p, t \in \mathcal{T}. \quad (4.8)$$

Nodal power injections are constrained due to generation and demand requirements as

$$\underline{p}_i^t \leq p_i^t \leq \bar{p}_i^t, \quad \forall i \in \mathcal{N}_p, t \in \mathcal{T}. \quad (4.9)$$

For power generators  $\bar{p}_i^t \geq \underline{p}_i^t \geq 0$  capture generation capacities or bids; for elastic loads  $\bar{p}_i^t \leq 0$ ; and for inelastic loads  $\underline{p}_i^t = \bar{p}_i^t \leq 0$  at all  $t \in \mathcal{T}$ .

Gas-fired generators constitute the links between the two infrastructures. A gas-fired generator sited on node  $i \in \mathcal{N}_g \cap \mathcal{N}_p$  withdraws gas  $\phi_i^t$  from the gas network and converts it to electric power  $p_i^t$ . The conversion is typically modeled by an affine heat-rate curve [57]:

$$-\phi_i^t = \beta_i p_i^t + \gamma_i, \quad \forall i \in \mathcal{N}_g \cap \mathcal{N}_p, t \in \mathcal{T} \quad (4.10)$$

described by the known parameters  $(\beta_i, \gamma_i)$ .

Based on the aforementioned modeling, the optimal gas power flow problem (OGPF) can be formally stated as the problem of minimizing the total cost of gas and power supply subject to the gas system (4.2)–(4.6), the power system (4.7)–(4.9), and the coupling constraints in (4.10), that is

$$\begin{aligned} \min \quad & \sum_{t \in \mathcal{T}} \left[ \sum_{i \in \mathcal{N}_p} b_i^t p_i^t + \sum_{i \in \mathcal{N}_g \setminus \mathcal{N}_p} a_i^t \phi_i^t \right] \\ \text{over} \quad & \{p_i^t, \theta_i^t\}_{i \in \mathcal{N}_p}, \{\phi_i^t, \pi_i^t\}_{i \in \mathcal{N}_g}, \{\phi_{ij}^t\}_{(i,j) \in \mathcal{L}_g}, \forall t \in \mathcal{T} \\ \text{s.to} \quad & (4.2) - (4.10). \end{aligned} \quad (4.11)$$

Both gas and power procurement costs are modeled as linear with corresponding coefficients (prices or bids)  $a_i^t$  and  $b_i^t$ . Note that the cost of running a gas-fired generator is accounted for as a power-related cost. Given the gas dynamics of (4.3), the gas flows and pressures that can be realized over  $\mathcal{T}$  depend on the initial gas system state  $\{\phi_{ij}^0\}_{(i,j) \in \mathcal{L}_g}$  and  $\{\pi_i^0\}_{i \in \mathcal{N}_g}$  that is included in the given problem parameters of (4.11).

Problem (4.11) minimizes a linear objective subject to affine (in)equalities and the quadratic equations in (3.6b). The latter constraints make (4.11) a non-convex quadratically constrained quadratic program (QCQP), and it thus hard to solve in general. Nevertheless, computational tasks pertaining to quadratic constraints have been successfully tackled using the powerful tool of feasible point pursuit (FPP) [29], with applications in power system operation among other fields [58]. The technique of FPP is adopted to tackle the OGPf next.

### 4.3 Feasible point pursuit-based solver

The OGPf can be posed as a QCQP upon replacing the quadratic equality (3.6b) by the two inequalities

$$(\pi_i^t)^2 \leq (\pi_j^t)^2 + \tilde{\mu}_{ij}(\phi_{ij}^t + \phi_{ji}^t)^2 \quad (4.12a)$$

$$(\pi_j^t)^2 + \tilde{\mu}_{ij}(\phi_{ij}^t + \phi_{ji}^t)^2 \leq (\pi_i^t)^2. \quad (4.12b)$$

By linearizing the RHS of (4.12) around  $(\check{\pi}_i^t, \check{\pi}_j^t, \check{\phi}_{ij}^t, \check{\phi}_{ji}^t)$  and upon introducing the slack variables  $(\delta_{ij}^t, \epsilon_{ij}^t)$ , the inequalities in (4.12) are replaced by

$$(\pi_i^t)^2 \leq \check{\pi}_j^t(2\pi_j^t - \check{\pi}_j^t) + \tilde{\mu}_{ij}(\check{\phi}_{ij}^t + \check{\phi}_{ji}^t)(2\phi_{ij}^t + 2\phi_{ji}^t - \check{\phi}_{ij}^t - \check{\phi}_{ji}^t) + \delta_{ij}^t \quad (4.13a)$$

$$(\pi_j^t)^2 + \tilde{\mu}_{ij}(\phi_{ij}^t + \phi_{ji}^t)^2 \leq \check{\pi}_i^t(2\pi_i^t - \check{\pi}_i^t) + \epsilon_{ij}^t. \quad (4.13b)$$

Adding the sum of the slack variables in the cost of the OGPf in (4.11) and replacing the

---

**Algorithm 2** Feasible point pursuit (FPP) algorithm
 

---

- 1: **Initialization:** Set  $k = 0$  and randomly initialize all the points in the set  $\mathcal{Z}(t)$ .
  - 2: Solve (4.14).
  - 3: Set  $\tilde{\pi}_i^t(k+1) = \pi_i^{t*}(k)$ ,  $\tilde{\pi}_j^t(k+1) = \pi_j^{t*}(k)$ ,  $\check{\phi}_{i,j}^t(k+1) = \phi_{ij}^{t*}(k)$  and  $\check{\phi}_{j,i}^t(k+1) = \phi_{ji}^{t*}(k)$ .
  - 4: Set  $k = k + 1$  **till convergence.**
- 

constraints in (4.3) with (4.13) leads to the optimization

$$\min \sum_{t \in \mathcal{T}} \left[ \sum_{i \in \mathcal{N}_p} b_i^t p_i^t + \sum_{i \in \mathcal{N}_g} a_i^t \phi_i^t + \kappa \sum_{(i,j) \in \mathcal{L}_g} (\delta_{ij}^t + \epsilon_{ij}^t) \right] \quad (4.14)$$

over  $\{\phi_i^t, \pi_i^t\}_{i \in \mathcal{N}_g}, \{p_i^t, \theta_i^t\}_{i \in \mathcal{N}_p}, \{\phi_{ij}^t, \delta_{ij}^t, \epsilon_{i,j}^t\}_{(ij) \in \mathcal{L}_g}, t \in \mathcal{T}$

s.to (4.2), (4.5) – (4.9), (4.13)

$$\delta_{ij}^t, \epsilon_{ij}^t \geq 0, \forall (i, j) \in \mathcal{N}_g.$$

Problem (4.14) is convex and can be solved using the FPP algorithm as explained in Algorithm 2. If the slack variables turn out to be zero, FPP is said to have converged to a KKT point [59], [29].

Note that the FPP algorithm solves a convex QCQP at every iteration. For a large system having more than 10 nodes where (4.14) is solved for 24 hours with time periods of one hour each, the number of variables is very large. Thus, a distributed algorithm using ADMM is required to solve each FPP iteration.

## 4.4 Distributed algorithm

The alternating direction method of multipliers (ADMM) algorithm solves convex optimization problems by partitioning the problem into smaller pieces, which are easier to handle. It enjoys the good convergence properties of method of multipliers and decomposability of dual decomposition [27]. For applications in the field of power systems see [33], [34]. In this section, ADMM is used to solve each iteration of problem (4.14). Furthermore, closed form solutions are obtained for select the ADMM subproblems.

It is known that ADMM can be very slow to converge to high accuracy. However, convergence to modest accuracy levels occurs within few iterations, which is acceptable for most practical applications [60] including optimal dispatch of coupled natural gas and power.

Applying ADMM to the optimal dispatch problem has the following advantages:

1. For every iteration of  $\mathbf{x}$ -update step in (2.6a), each node and pipeline only need to solve a local subproblem.
2. Communication is required only between a node and the pipeline segments connected to the node.
3. There is a closed-form solution for the  $\mathbf{y}$ -update step in (2.6b).

Consider partitioning the coupled gas and power system into  $|\mathcal{N}_g|$  nodal areas and  $|\mathcal{L}_g|$  pipeline segment areas and one power system area. Each node  $i \in \mathcal{N}_g \setminus \mathcal{N}_g \cap \mathcal{N}_p$  is an agent

represented by  $A_i$ . The variables maintained by the agent  $A_i$  belong to the set  $\mathcal{A}_i$  defined as

$$\mathcal{A}_i := \{\pi_i^t, \phi_i^t, \phi_{ij}^t\}_{j \in \mathcal{N}_i, t \in \mathcal{T}}$$

where  $\mathcal{N}_i$  is a set of all the nodes adjacent to  $i$ .

Every node  $i$  belonging to the set  $\mathcal{N}_g \cap \mathcal{N}_p$  is an agent represented by  $B_i$ , which holds the variables belonging to the set  $\mathcal{B}_i$  defined as

$$\mathcal{B}_i := \{\pi_i^t, \phi_i^t, \phi_{ij}^t, p_i^t\}_{j \in \mathcal{N}_i, t \in \mathcal{T}}.$$

Similar to the nodal agents, the variables maintained by each pipeline agent  $C_{ij}$  for all  $(i, j) \in \mathcal{L}_g \setminus \mathcal{L}_a$  belong to the set  $\mathcal{C}_{ij}$  as follows

$$\mathcal{C}_{ij} := \{\phi_{ij}^t, \phi_{ji}^t, \pi_i^t, \pi_j^t, \delta_{ij}^t, \epsilon_{ij}^t\}_{t \in \mathcal{T}}.$$

For an active pipeline  $(i, j) \in \mathcal{L}_a$ , define another agent denoted by  $D_{i,j}$  that maintains the variables belonging to the set  $\mathcal{D}_{i,j}$  as shown

$$\mathcal{D}_{ij} := \{\pi_i^t, \pi_j^t\}_{t \in \mathcal{T}}.$$

Finally, all the variables corresponding to the power system are maintained by a single agent denoted by  $E$ . The variables held by  $E$  belong to the set  $\mathcal{E}$ , which is defined as

$$\mathcal{E} := \{p_i^t, \theta_i^t\}_{t \in \mathcal{T}}.$$

Note that the sets  $\mathcal{A}_i$ ,  $\mathcal{B}_i$ ,  $\mathcal{C}_{ij}$ ,  $\mathcal{D}_{ij}$  and  $\mathcal{E}$  have partial overlapping, which is illustrated in Fig 4.2.

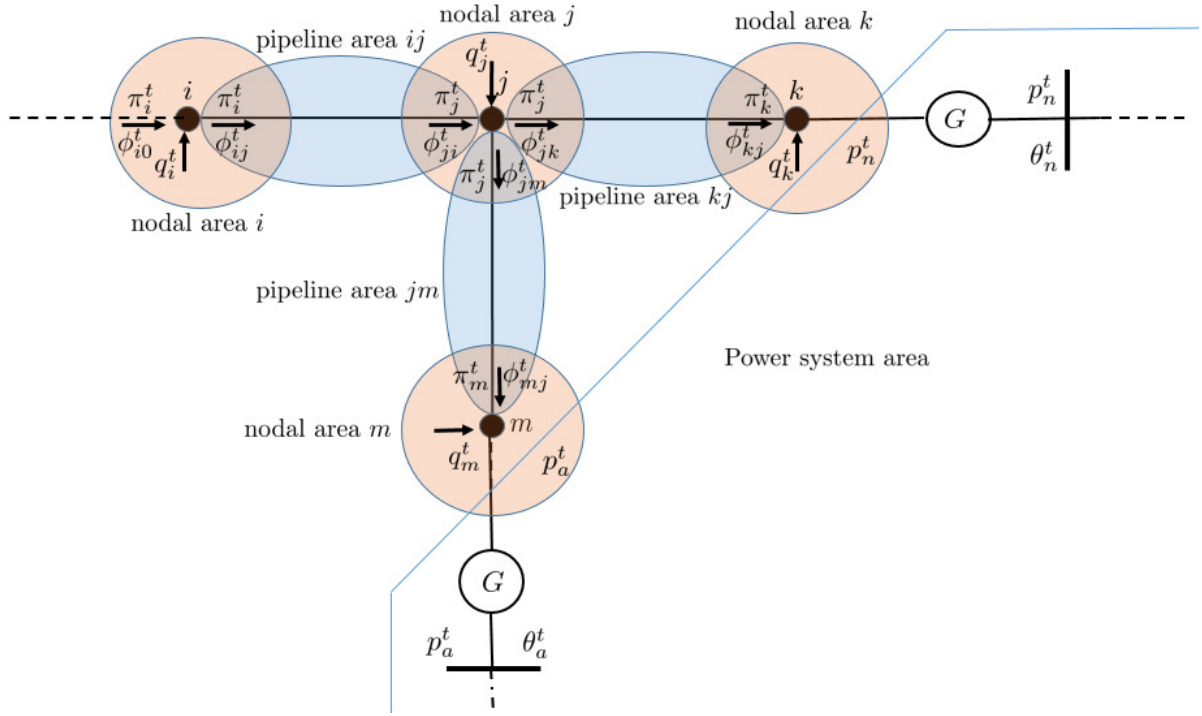


Figure 4.2: Overlapping between different areas.

To enable a truly decentralized solution, an auxiliary variable is introduced per pair of shared variables (variables lying in the overlapping regions), as follows:

$$\pi_i^t(\mathcal{A}_i) = \hat{\pi}_i^t, \quad (4.15a)$$

$$\pi_i^t(\mathcal{C}_{i,j}) = \hat{\pi}_i^t, \quad (4.15b)$$

$$\pi_i^t(\mathcal{B}_i) = \hat{\pi}_i^t, \quad (4.15c)$$

$$\pi_i^t(\mathcal{D}_{ij}) = \hat{\pi}_i^t, \quad (4.15d)$$

$$\phi_{ij}^t(\mathcal{A}_i) = \hat{\phi}_{ij}^t, \quad (4.15e)$$

$$\phi_{ij}^t(\mathcal{B}_i) = \hat{\phi}_{ij}^t, \quad (4.15f)$$

$$\phi_{ij}^t(\mathcal{C}_{ij}) = \hat{\phi}_{ij}^t, \quad (4.15g)$$

---

**Algorithm 3** FPP and ADMM
 

---

- 1: **Initialization:** Set  $k = 0$  and randomly initialize all the points in the set  $\mathcal{Z}(t)$ .
  - 2: Solve (4.16), (4.17), (4.18), (4.20) and (4.21).
  - 3: Perform the  $\mathbf{y}$ -update step and Lagrange multiplier step described in (2.6b) and (2.6c), respectively.
  - 4: Set  $\tilde{\pi}_i^t(k+1) = \pi_i^{t*}(k)$ ,  $\tilde{\pi}_j^t(k+1) = \pi_j^{t*}(k)$ ,  $\check{\phi}_{i,j}^t(k+1) = \phi_{ij}^{t*}(k)$  and  $\check{\phi}_{j,i}^t(k+1) = \phi_{ji}^{t*}(k)$ .
  - 5: Set  $k = k + 1$  **till convergence**.
- 

$$\phi_{ji}^t(\mathcal{C}_{ji}) = \hat{\phi}_{ji}^t, \quad (4.15h)$$

$$p_i^t(\mathcal{B}_i) = \hat{p}_i^t, \quad \forall i \in \mathcal{N}_g \cap \mathcal{N}_p \quad (4.15i)$$

$$p_i^t(\mathcal{E}) = \hat{p}_i^t, \quad \forall i \in \mathcal{N}_g \cap \mathcal{N}_p. \quad (4.15j)$$

where the term in parenthesis indicates the set in which the variable belongs to. For notational brevity, the parenthesis is ignored later in the text and the variable set is understood from context.

The next step is to decouple the optimization problem in (4.14) and write optimization subproblems for each agent. To that end, define Lagrange multipliers  $\lambda_i^{1,t}$ ,  $\lambda_i^{2,t}$ ,  $\lambda_i^{3,t}$ ,  $\lambda_i^{4,t}$ ,  $\lambda_{ij}^{1,t}$ ,  $\lambda_{ij}^{2,t}$ ,  $\lambda_{ij}^{3,t}$ ,  $\lambda_{ji}^{3,t}$ ,  $\lambda_i^{4,t}$  and  $\lambda_i^{5,t}$  corresponding to equations (4.15a)–(4.15j), respectively.

According to (2.6a), each nodal agent  $\{A_i\}_{i \in \mathcal{N}_g \setminus \mathcal{N}_g \cap \mathcal{N}_p}$  solves the following minimization problem for all  $t \in \mathcal{T}$ :

$$\min a_i^t \phi_i^t + \frac{\rho_1}{2} (\pi_i^t - \hat{\pi}_i^t + \lambda_i^{1,t})^2 + \frac{\rho_2}{2} \sum_{j \in \mathcal{N}_i} (\phi_{ij}^t - \hat{\phi}_{ij}^t + \lambda_{ij}^{1,t})^2 \quad (4.16)$$

$$\text{over } \phi_i^t, \phi_{ij}^t, \pi_i^t$$

s.to (4.2), (4.4), (4.5)

Similarly, for all  $t \in \mathcal{T}$  each agent  $\{B_i\}_{i \in \mathcal{N}_g \cap \mathcal{N}_p}$  solves:

$$\min \frac{\rho_3}{2}(p_i^t - \hat{p}_i^t + \lambda_i^{5,t})^2 + \frac{\rho_4}{2}(\pi_i^t - \hat{\pi}_i^t + \lambda_i^{3,t})^2 + \frac{\rho_5}{2} \sum_{j \in N_i} (\phi_{ij}^t - \hat{\phi}_{ij}^t + \lambda_{ij}^{2,t})^2 \quad (4.17)$$

over  $\phi_i^t, \phi_{ij}^t, \pi_i^t$

s.to (4.2), (4.4), (4.5), (4.10)

The agent  $C_{ij}$  corresponding to the non-active pipeline  $(i, j) \in \mathcal{L}_g \setminus \mathcal{L}_a$ , tackles the following optimization problem:

$$\min \frac{\rho_6}{2}(\pi_i^t - \hat{\pi}_i^t + \lambda_i^{2,t})^2 + \frac{\rho_7}{2} \sum_{j \in N_i} (\phi_{ij}^t - \hat{\phi}_{ij}^t + \lambda_{ij}^{3,t})^2 + \quad (4.18)$$

$$\frac{\rho_8}{2} \sum_{j \in N_i} (\phi_{ji}^t - \hat{\phi}_{ji}^t + \lambda_{ji}^{3,t})^2 + \kappa \sum_{j \in N_i} (\delta_{ij}^t + \epsilon_{ij}^t) \quad (4.19)$$

over  $\phi_{ij}^t, \phi_{ji}^t, \pi_i^t, \delta_{ij}^t, \epsilon_{ij}^t$

s.to  $\delta_{ij}^t, \epsilon_{ij}^t \geq 0$ , (4.3)

The active pipeline agent  $\{\mathcal{D}_{ij}\}_{(i,j) \in \mathcal{L}_a}$  seeks to solve the following minimization problem for all  $t \in \mathcal{T}$ :

$$\min \frac{\rho_8}{2}(\pi_i^t - \hat{\pi}_i^t + \lambda_i^{4,t})^2 \quad (4.20)$$

over  $\pi_i^t, \pi_j^t$

s.to (4.6)

Finally, for all  $t \in \mathcal{T}$ , agent  $\mathcal{E}$  handles the below mentioned minimization problem:

$$\begin{aligned} \min \quad & b_i^t p_i^t + \frac{\rho_9}{2} (p_i^t - \hat{p}_i^t + \lambda_i^{5,t})^2 \\ \text{over } & p_i^t, \theta_i^t \\ \text{s.to } & (4.7) - (4.9). \end{aligned} \tag{4.21}$$

Note that  $\{\rho_n\}_{n=1}^9$  are positive constants.

In general, the auxiliary variable update step or the  $\mathbf{y}$ -update step described in (2.6b) handles optimization problem of the form:

$$\min_y (y - \hat{y} + \lambda_1)^2 + (y - \tilde{y} + \lambda_2)^2,$$

where  $\lambda_1$  and  $\lambda_2$  are variables corresponding to (2.6c). Taking derivative with respect to  $y$  and equating it to zero yields

$$y^* = \frac{\hat{y} + \tilde{y} - \lambda_1 - \lambda_2}{2}. \tag{4.22}$$

From equations (2.6b) and (2.6c), it is easy to verify that  $\lambda_1 + \lambda_2 = 0$ . Thus, the minimizer  $y^*$  has the closed-form expression  $y^* = \frac{1}{2}(\hat{y} + \tilde{y})$ .

The auxiliary variables defined in (4.15) are updated using the aforementioned closed-form expression and the Lagrange multipliers are updated according to (2.6c).

## 4.5 Numerical tests

The developed FPP and ADMM approaches for solving optimal dispatch problem were tested on a part of the Belgian natural gas network [3], coupled with the 14-bus IEEE benchmark

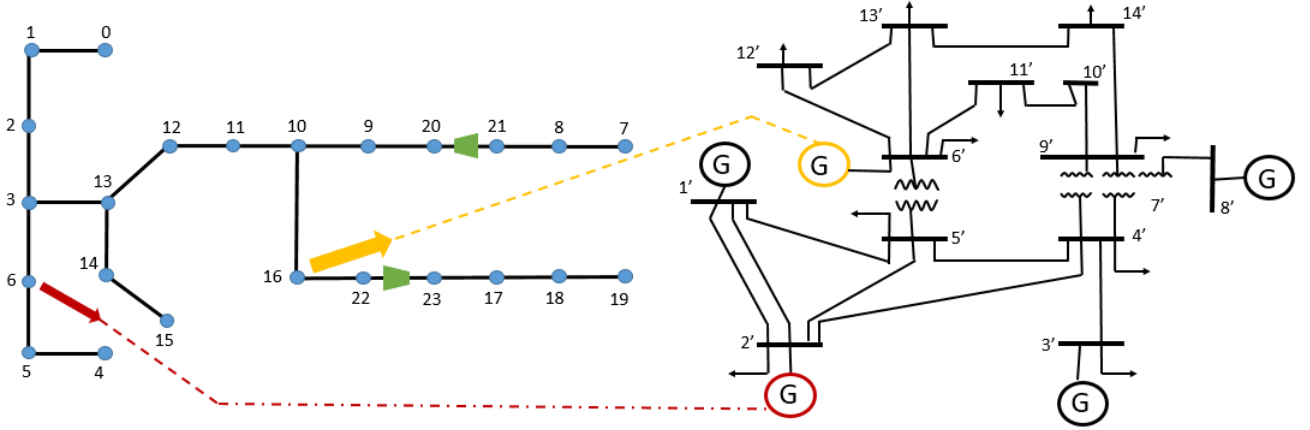


Figure 4.3: Coupled gas and power system network. Red and yellow arrows indicate gas flow from the gas network to the gas fired generator connected to the power network.

power network as shown in Fig. 4.3. The gas network contains 24 nodes connected with 21 passive and 2 active pipelines, two of which are active ones with compressor ratios equal to 1.5. Although the original network contains loops, its publicized version has been simplified to a tree. The power network is radial and is connected to gas network via gas fired generators placed at nodes 5 and 12. All FPP and ADMM problems were solved on a laptop with a 3.1 GHz Intel Core i7 processor with 16GB RAM using the SDPT3 solver in YALMIP [48], [49].

At first, nominal nodal gas and power demands were set to fixed values taken from the data provided in [3] and the IEEE 14-bus power system benchmark data, respectively. The variation in gas and power demand at nodes with respect to time can be seen in Fig 4.4 and Fig 4.4, respectively. For every one hour, several different realistic demand profiles were created by increasing or decreasing the demands at various gas and power system nodes such. For implementing the FPP algorithm, the points  $\check{\pi}_i^t, \check{\pi}_j^t, \check{\phi}_{ij}^t, \check{\phi}_{ji}^t$  were initialized at 0 and the

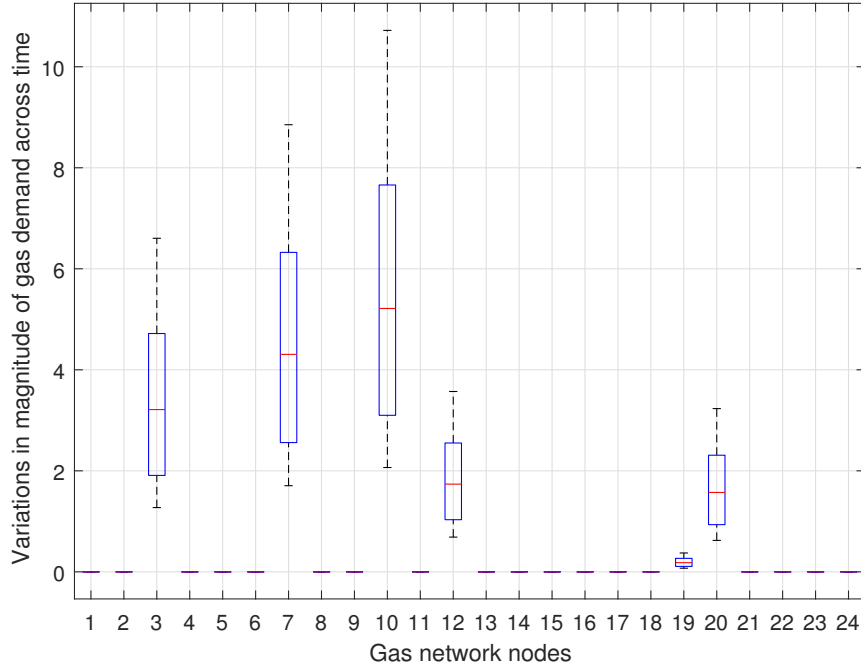


Figure 4.4: Gas demand profiles.

iteration index was set to  $k = 0$ . Given nodal demands and the pressure at the reference node, flows, gas and power injections and the voltage phase were found after solving problem (4.14) as per the Algorithm 2. The FPP algorithm converges in a few iterations as shown in Fig. 4.6.

Having solved the optimal dispatch problem using FPP-based approach, we then tested the distributed implementation devised in Section 4.4. The auxiliary variables  $\hat{\pi}_i^t$ ,  $\hat{\phi}_{i,j}^t$ ,  $\hat{p}_i^t$ , and the Lagrange multipliers  $\lambda_i^{1,t}$ ,  $\lambda_i^{2,t}$ ,  $\lambda_i^{3,t}$ ,  $\lambda_i^{4,t}$ ,  $\lambda_{i,j}^{1,t}$ ,  $\lambda_{i,j}^{2,t}$ ,  $\lambda_{i,j}^{3,t}$ ,  $\lambda_i^{4,t}$ ,  $\lambda_i^{5,t}$  and  $\lambda_i^{6,t}$  were set to 0 at the beginning of every iteration of FPP. Given the previously generated demand profiles and reference node pressure each iteration of FPP was solved using ADMM. The obtained values

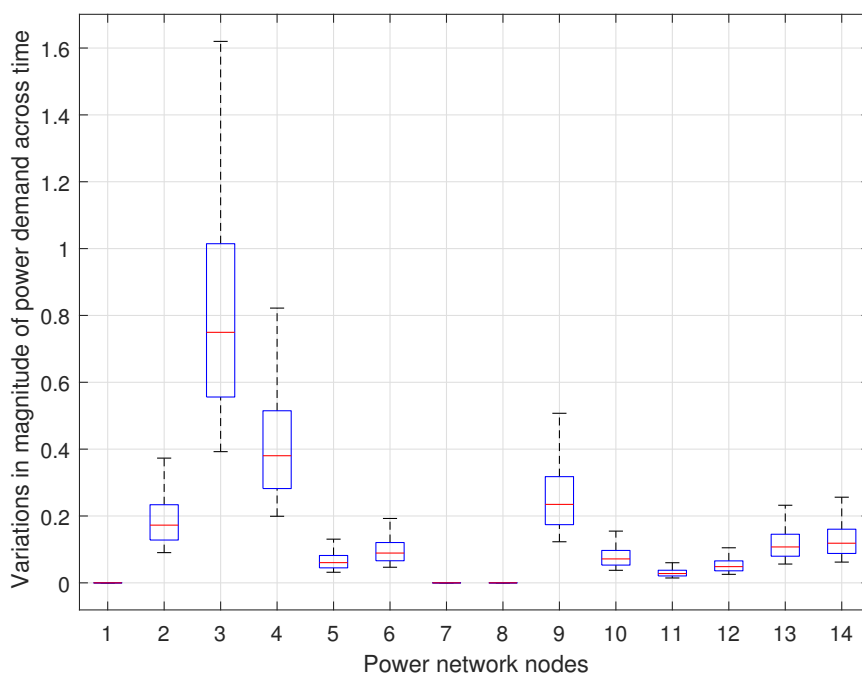


Figure 4.5: Gas demand profiles.

of pressure, flows, voltage phase and power demands match the results of FPP algorithm. The gas flow out of node 16 and power generated by the generator connected at node 16 of the gas network is shown in Fig. 4.7, which corroborates to the fact that the relationship is affine. The pressure variations at the nodes containing the gas-fired generators is shown in Fig. 4.8. The developed FPP+ADMM approach works on large networks with thousand of nodes, while its performance improves with better initial point selection.

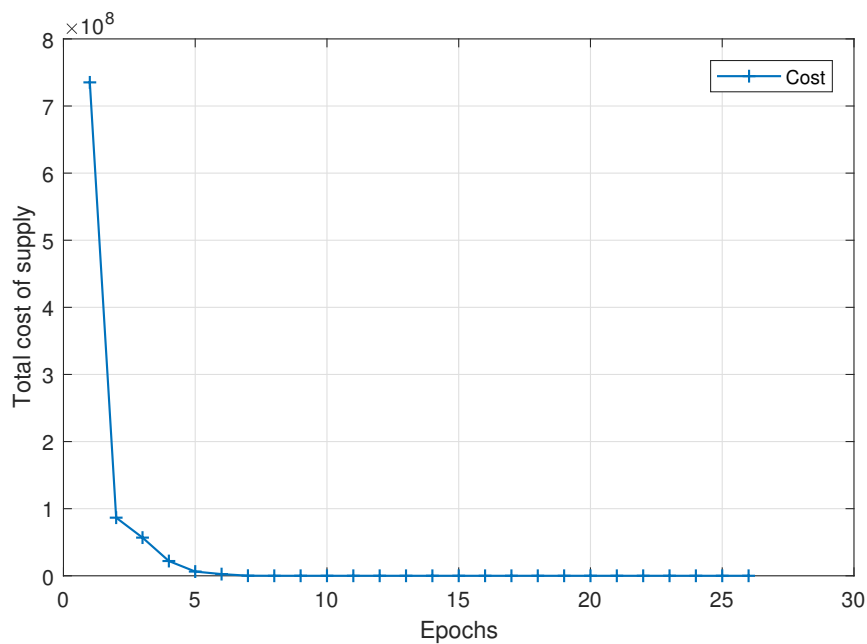


Figure 4.6: Convergence plot for FPP algorithm.

## 4.6 Conclusion

The optimal dispatch problem for coupled natural gas and electric power system infrastructures has been posed as a convex minimization problem. It has been solved using the FPP algorithm, which converges in a few iterations. For addressing the need to solve optimal dispatch for large networks, distributed algorithm has been developed using ADMM. The developed computational toolbox helps in understanding the dynamics and modeling the coupling between natural gas and the electric grid infrastructures.

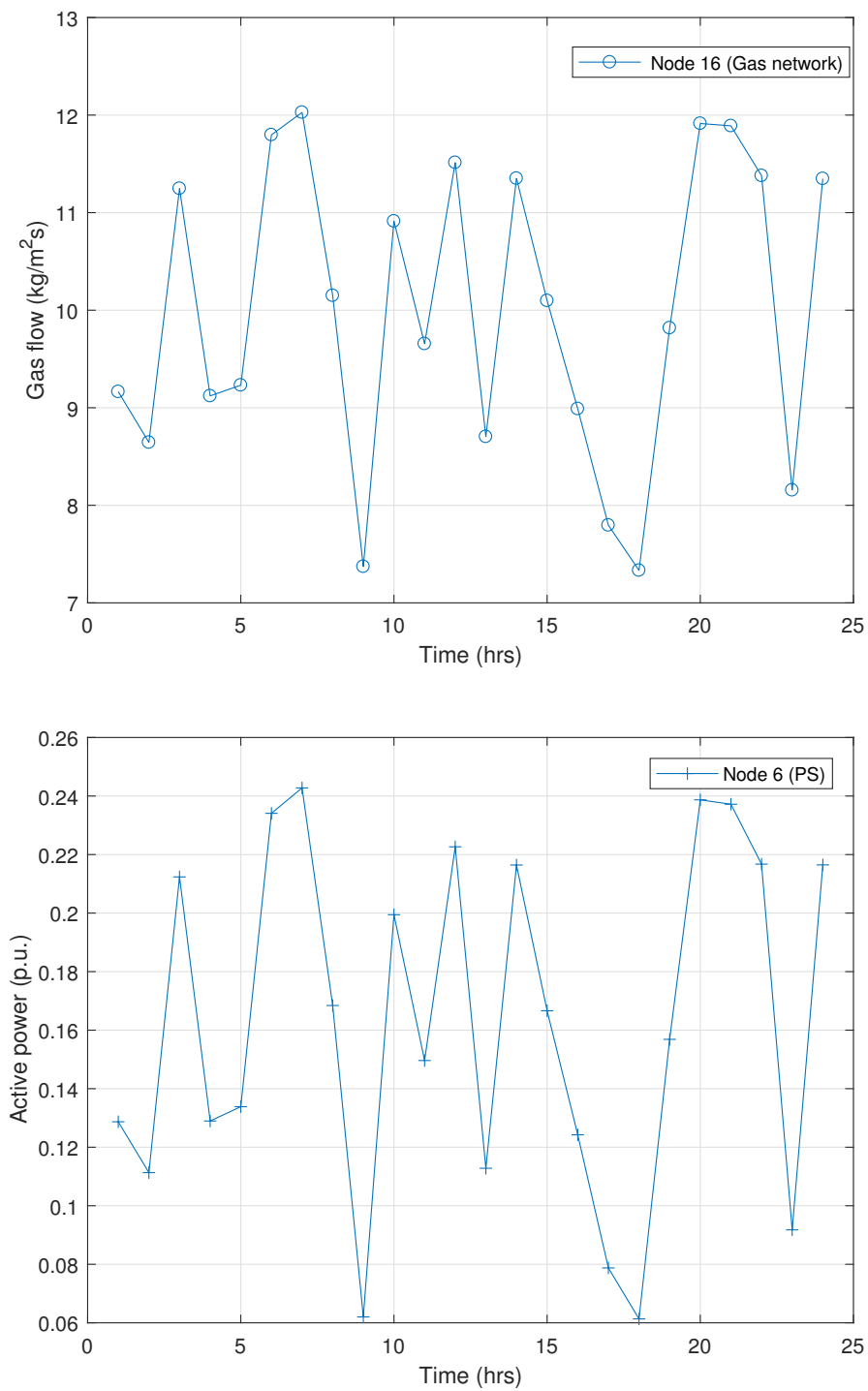


Figure 4.7: a) Gas flow out of node 16 of the gas network. b) Power generator by the gas-fired generator at node 16 of the gas network

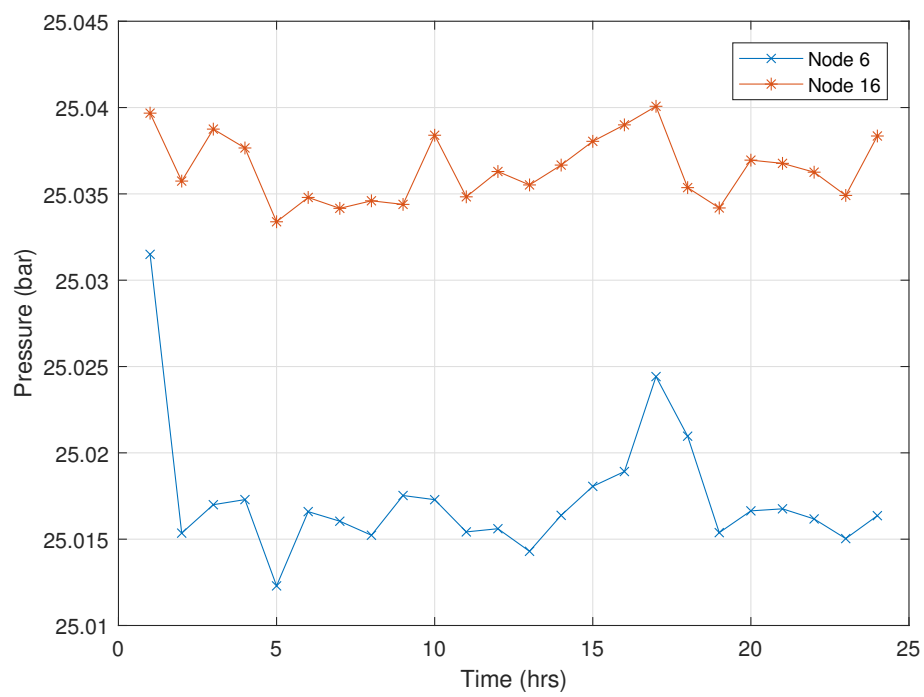


Figure 4.8: Pressure at gas power nodes.

# Bibliography

- [1] Energy Information Administration, “About U.S. Natural Gas Pipelines - Transporting Natural Gas,” 2008. [Online]. Available: [https://www.eia.gov/pub/oil\\_gas/natural\\_gas/analysis\\_publications/ngpipeline/transcorr\\_map.html](https://www.eia.gov/pub/oil_gas/natural_gas/analysis_publications/ngpipeline/transcorr_map.html)
- [2] I. D. S. F. Joao, S. O. Alexandre, F. P. F. Luis, C. M. Mauricio, D. V. G. Jose, de Melo Camargo, R. d. S. Marcos, and R. Alexandre, “Electric Power System Operation Decision Support by Expert System Built with Paraconsistent Annotated Logic,” 2012. [Online]. Available: <https://www.intechopen.com/books/advances-in-expert-systems/>
- [3] D. De Wolf and Y. Smeers, “Optimal dimensioning of pipe networks with application to gas transmission networks,” *Operations Research*, vol. 44, no. 4, pp. 596–608, Jul. 1996.
- [4] “Fluxy’s Belgium Transmission network,” Fluxy, Tech. Rep. [Online]. Available: <http://www.fluxys.com/belgium/en/about%20fluxys/infrastructure/network/network>
- [5] S. Misra, M. W. Fisher, S. Backhaus, R. Bent, M. Chertkov, and F. Pan, “Optimal compression in natural gas networks: A geometric programming approach,” *IEEE Trans.*

- Control of Network Systems*, vol. 2, no. 1, pp. 47–56, Mar. 2015.
- [6] “The future of natural gas: MIT energy initiative,” Massachusetts Institute of Technology, Tech. Rep., 2011. [Online]. Available: <http://energy.mit.edu/wp-content/uploads/2011/06/MITEI-The-Future-of-Natural-Gas.pdf>
- [7] R. Rubio, D. Ojeda-Esteybar, O. Ano, and A. Vargas, “Integrated natural gas and electricity market: A survey of the state of the art in operation planning and market issues,” in *IEEE/PES Transmission and Distribution Conf. and Exposition*, Aug. 2008.
- [8] A. Zlotnik, L. Roald, S. Backhaus, M. Chertkov, and G. Andersson, “Coordinated scheduling for interdependent electric power and natural gas infrastructures,” *IEEE Transactions on Power Systems*, vol. 32, no. 1, pp. 600–610, 2017.
- [9] T. T. C. T. Leung, “Coupled natural gas and electric power systems,” Ph.D. dissertation, Massachusetts Institute of Technology, 2015.
- [10] “Design of wholesale electricity markets,” Electric Power Research Institute, Tech. Rep.
- [11] J. J. Maugis, “Design and operation of gas transmission networks,” *Etude de reseaux de transport et de distribution de fluide*, vol. 11, no. 2, pp. 243–248, 1977.
- [12] A. Martinez-Mares and C. R. Fuerte-Esquivel, “Integrated energy flow analysis in natural gas and electricity coupled systems,” in *Proc. North American Power Symposium*, Boston, MA, Aug. 2011.

- [13] K. Dvijotham, M. Vuffray, S. Misra, and M. Chertkov, “Natural gas flow solutions with guarantees: A monotone operator theory approach,” submitted 2015. [Online]. Available: <http://arxiv.org/abs/1506.06075>
- [14] A. Ojha, V. Kekatos, and R. Baldick, “Solving the natural gas flow problem using semidefinite program relaxation,” in *Proc. IEEE Power & Energy Society General Meeting*, Chicago, IL, 2016.
- [15] F. Babonneau, Y. Nesterov, and J.-P. Vial, “Design and operation of gas transmission networks,” *Operations Research*, vol. 60, no. 1, pp. 34–47, Feb. 2012.
- [16] S. Wu, L. R. Scott, and E. A. Boyd, “Towards the simplification of natural gas transmission networks,” in *Proc. NSF Design and Manufacturing Grantees Conference*, Long Beach, CA, Jan. 1999.
- [17] E. K. Ryu and S. Boyd, “A primer on monotone operator methods,” *Appl. Comput. Math.*, vol. 15, no. 1, pp. 3–43, Nov. 2016.
- [18] M. Chaudry, N. Jenkins, and G. Strbac, “Multi-time period combined gas and electricity network optimisation,” *Electric Power Systems Research*, vol. 78, no. 7, pp. 1265–1279, 2008.
- [19] S. Jenkins, A. Annaswamy, J. Hansen, and J. Knudsen, “A dynamic model of the combined electricity and natural gas markets,” in *Proc. IEEE Conf. on Innovative Smart Grid Technologies*, Washington, DC, Feb. 2016.

- [20] M. Chertkov, S. Backhaus, R. Bent, and S. Misra, “Pressure fluctuations in natural gas networks caused by gas-electric coupling,” in *Proc. IEEE Hawaii Intl. Conf. on System Sciences*, Kauai, HI, Jan. 2015.
- [21] C. Wang, W. Wei, J. Wang, L. Bai, and Y. Liang, “Distributed optimal gas-power flow using convex optimization and ADMM,” 2016, (submitted). [Online]. Available: <https://arxiv.org/abs/1610.04681>
- [22] M. Farivar and S. Low, “Branch flow model: Relaxations and convexification — Part I,” *IEEE Trans. Power Syst.*, vol. 28, no. 3, pp. 2554–2564, Aug. 2013.
- [23] T. Lipp and S. Boyd, “Variations and extension of the convex–concave procedure,” *Optimization and Engineering*, vol. 17, no. 2, pp. 263–287, 2016.
- [24] S. Boyd, N. Parikh, E. Chu, B. Peleato, and J. Eckstein, “Distributed optimization and statistical learning via the alternating direction method of multipliers,” *Found. Trends Mach. Learning*, vol. 3, pp. 1–122, 2010.
- [25] C. M. Correa-Posada and P. Sánchez-Martin, “Security-constrained optimal power and natural-gas flow,” *IEEE Trans. Power Syst.*, vol. 29, no. 4, pp. 1780–1787, Jul. 2014.
- [26] L. Vandenberghe and S. Boyd, “Semidefinite programming,” *SIAM review*, vol. 38, no. 1, pp. 49–95, 1996.
- [27] S. Boyd and L. Vandenberghe, *Convex Optimization*. New York, NY: Cambridge University Press, 2004.

- [28] Z.-Q. Luo, W.-K. Ma, A. M.-C. So, Y. Ye, and S. Zhang, “Semidefinite relaxation of quadratic optimization problems,” *IEEE Signal Processing Mag.*, vol. 27, no. 3, pp. 20–34, 2010.
- [29] O. Mehanna, K. Huang, B. Gopalakrishnan, A. Konar, and N. D. Sidiropoulos, “Feasible point pursuit and successive approximation of non-convex qcqps,” *IEEE Signal Processing Letters*, vol. 22, no. 7, pp. 804–808, 2015.
- [30] J. Douglas and H. H. Rachford, “On the numerical solution of heat conduction problems in two and three space variables,” *Transactions of the American mathematical Society*, vol. 82, no. 2, pp. 421–439, 1956.
- [31] P. L. Lions and B. Mercier, “Splitting algorithms for the sum of two nonlinear operators,” *SIAM Journal on Numerical Analysis*, vol. 16, no. 6, pp. 964–979, 1979.
- [32] J. Eckstein and D. P. Bertsekas, “On the douglas—rachford splitting method and the proximal point algorithm for maximal monotone operators,” *Mathematical Programming*, vol. 55, no. 1, pp. 293–318, 1992.
- [33] P. Šulc, S. Backhaus, and M. Chertkov, “Optimal distributed control of reactive power via the alternating direction method of multipliers,” *IEEE Transactions on Energy Conversion*, vol. 29, no. 4, pp. 968–977, 2014.
- [34] V. Kekatos and G. B. Giannakis, “Distributed robust power system state estimation,” *IEEE Transactions on Power Systems*, vol. 28, no. 2, pp. 1617–1626, 2013.

- [35] Q. Peng and S. H. Low, “Distributed optimal power flow algorithm for balanced radial distribution networks,” *arXiv preprint arXiv:1404.0700*, 2015.
- [36] Crane Company, “Flow of fluids through valves, fittings, and pipe,” Engineering Division, Tech. Rep., 1979.
- [37] A. Osiadacz, *Simulation and analysis of gas networks*. Gulf Publishing, 1987.
- [38] A. Thorley and C. Tiley, “Unsteady and transient flow of compressible fluids in pipelines – a review of theoretical and some experimental studies,” *Intl. Journal of Heat and Fluid Flow*, vol. 8, no. 1, pp. 3–15, Mar. 1987.
- [39] M. X. Goemans and D. P. Williamson, “Improved approximation algorithms for maximum cut and satisfiability problem using semi-definite programming,” *Journal of the ACM*, vol. 42, pp. 1115–1145, 1995.
- [40] X. Bai, H. Wei, K. Fujisawa, and Y. Yang, “Semidefinite programming for optimal power flow problems,” *Intl. Journal of Electric Power & Energy Systems*, vol. 30, no. 6, pp. 383–392, 2008.
- [41] H. Zhu and G. B. Giannakis, “Power system nonlinear state estimation using distributed semidefinite programming,” *IEEE J. Sel. Topics Signal Process.*, vol. 8, no. 6, pp. 1039–1050, Dec. 2014.
- [42] E. J. Candes, Y. C. Eldar, T. Strohmer, and V. Voroninski, “Phase retrieval via matrix completion,” *SIAM Journal on Imaging Sciences*, vol. 6, no. 1, pp. 199–225, 2013.

- [43] R. Madani, J. Lavaei, and R. Baldick, “Convexification of power flow problem over arbitrary networks,” in *Proc. IEEE Conf. on Decision and Control*, Osaka, Japan, Dec. 2015.
- [44] Y. Zhang, R. Madani, and J. Lavaei, “Power system state estimation with line measurements,” 2016, submitted. [Online]. Available: [https://www.ocf.berkeley.edu/~yuzhang/SE\\_Line\\_2016.pdf](https://www.ocf.berkeley.edu/~yuzhang/SE_Line_2016.pdf)
- [45] W. T. Tutte, “The factorization of linear graphs,” *Journal of the London Mathematical Society*, vol. 22, no. 2, pp. 107–111, 1947.
- [46] F. Alizadeh, J.-P. A. Haeberly, and M. L. Overton, “Complementarity and nondegeneracy in semidefinite programming,” *Mathematical programming*, vol. 77, no. 1, pp. 111–128, Apr. 1997.
- [47] L. Vandenberghe and S. Boyd, “Semidefinite programming,” *SIAM Review*, vol. 38, no. 1, pp. 49–95, Mar. 1996.
- [48] R. H. Tutuncu, K. C. Toh, and M. Todd, “Solving semidefinite-quadratic-linear programs using SDPT3,” *Mathematical Programming Ser. B*, vol. 95, pp. 189–217, 2003.
- [49] J. Lofberg, “A toolbox for modeling and optimization in MATLAB,” in *Proc. of the CACSD Conf.*, 2004. [Online]. Available: <http://users.isy.liu.se/johanl/yalmip/>

- [50] R. Ríos-Mercado and Z. Roger, “Natural gas pipeline optimization,” in *Handbook of Applied Optimization*, P. Pardalos and M. Resende, Eds. Oxford University Press, 2002, pp. 813–825.
- [51] C. M. Correa-Posada and P. Sánchez-Martín, “Integrated power and natural gas model for energy adequacy in short-term operation,” *IEEE Transactions on Power Systems*, vol. 30, no. 6, pp. 3347–3355, 2015.
- [52] A. Tomasgard, F. Rømo, M. Fodstad, and K. Midthun, “Optimization models for the natural gas value chain,” in *Geometric modelling, numerical simulation, and optimization*. Springer, 2007, pp. 521–558.
- [53] A. Zlotnik, M. Chertkov, and S. Backhaus, “Optimal control of transient flow in natural gas networks,” in *Proc. IEEE Conf. on Decision and Control*, Osaka, Japan, Dec. 2015, pp. 4563–4570.
- [54] T. Li, M. Eremia, and M. Shahidehpour, “Interdependency of natural gas network and power system security,” *IEEE Trans. Power Syst.*, vol. 23, no. 4, pp. 1817–1824, Nov. 2008.
- [55] C. Liu, M. Shahidehpour, M. Fu, and Z. Li, “Security-constrained unit commitment with natural gas transmission constraints,” *IEEE Trans. Power Syst.*, vol. 24, no. 3, pp. 1523–1536, Aug. 2009.
- [56] M. Chaudry, J. Wu, and N. Jenkins, “A sequential monte carlo model of the combined gb gas and electricity network,” *Energy Policy*, vol. 62, pp. 473–483, 2013.

- [57] J. B. Klein *et al.*, “The use of heat rates in production cost modeling and market modeling,” 1998.
- [58] G. Wang, A. Zamzam, G. Giannakis, N. Sidiropoulos, and J. Chen, “Power system state estimation via feasible point pursuit: Algorithms and cramer-rao bound,” *IEEE Transactions on Power Systems*, 2017, (submitted).
- [59] A. Beck, A. Ben-Tal, and L. Tetrushvili, “A sequential parametric convex approximation method with applications to nonconvex truss topology design problems,” *Journal of Global Optimization*, vol. 47, no. 1, pp. 29–51, 2010.
- [60] S. Boyd, N. Parikh, E. Chu, B. Peleato, and J. Eckstein, “Distributed optimization and statistical learning via the alternating direction method of multipliers,” *Foundations and Trends® in Machine Learning*, vol. 3, no. 1, pp. 1–122, 2011.